ISO/FIRST Glitches Working Group

Final Report

Issue 1.1

21 August 2001

Document Information

Document Title: ISO/FIRST Glitches Working Group Final Report

Reference Number: SAI/2001-013/Rp

Issue: Issue 1.1

Issue Date: 21 August 2001

Authors: Glitches Working Group

Editor: Ana M. Heras

Document Change Record

ISO/FIRST Glitches Working Group Final Report

Date	Revision	Comments
15 November 2000	Draft 1.0	First draft
25 July 2001	Issue 1.0	Document issued
21 August 2001	Issue 1.1	Sections 4.2 and 4.4 modified

Contents

1. Introduction

1.1 Purpose of the document

The purpose of this document is to provide a comprehensive report on the space radiation effects on the ISO instruments and how these effects are handled in the reduction of the ISO data. In addition the document contains the initial studies for prediction of the radiation effects in the FIRST satellite (recently renamed as Herschel Space Observatory), in particular the PACS instrument, and provides recommendations for future missions.

Most of the work presented here is the result of the ISO/FIRST Glitches Working Group (GWG). Relevant information from other sources has also been included in order to provide a complete overview. This external information has been flagged in the document, providing the corresponding references.

1.2 Structure of the document

The document is a compilation of the work carried out by the GWG. For each topic and instrument, an introduction to the problem is given, followed by a presentation of the results obtained and the conclusions. In order to limit the extension of the report and still to provide all the information available, each section contains the corresponding hyperlinks to Web pages, documents and published papers in which a more detailed description of the study and the results can be found. These hyperlinks are active allowing the reader to display the document through the Web at any time. If the reader prefers to download all the documents belonging to this report and print them at his/her convenience, a gzipped tar file is available here.

The authorship of text extracted from documents or papers is given in the hyperlink/reference. Sections in which the author is not explicitly mentioned have been contributed by the GWG member responsible for that particular area, as listed in section 1.3.2.

1.3 The ISO/FIRST Glitches Working Group

1.3.1 Objectives

The objectives of the of the ISO/FIRST Glitches Working Group are:

- To provide statistics of the radiation effects on the ISO instruments (glitch counts, glitch height distributions), compare the results between instruments and detector types and correlate the observed glitches with the space weather.

- To model the radiation effects on the ISO detectors and compare with the observations, in order to improve our understanding of the radiation environment, and the effects of detector geometry and shielding.

- To characterize the type of glitches observed in each detector type.

- To improve the deglitching and detailing algorithms in the ISO data reduction packages, that is, Interactive Analysis (IA) and Off Line Processing (OLP).

- To analyse the space radiation environment to be encountered by FIRST (Herschel) and perform the first simulation of the radiation effects on the PACS detectors.

- Compile and transfer space radiation effects knowledge based on the ISO experience to future missions.

1.3.2 GWG Members

The ISO/FIRST Glitches Working Group members are:

Babar Ali (USA ISO User support)

Infrared Processing and Analysis Center, Caltech, Mail Code 100-22, 770 S. Wilson Avenue, Pasadena, CA 91125, USA

babar@ipac.caltech.edu

Martin Burgdorf (LWS)

ISO Data Centre, Astrophysics Division, Space Science Department of ESA, Villafranca del Castillo, P.O. Box 50727, 28080-Madrid, Spain

mburgdor@iso.vilspa.esa.es

Arnaud Claret (ISOCAM)

Service d'Astrophysique, CEA/DSM/DAPNIA Saclay, Orme des Merisiers, 91191 Gif-sur-Yvette Cédex, France

claret@discovery.saclay.cea.fr

Herve Dzitko (ISOCAM)

Service d'Astrophysique, CEA/DSM/DAPNIA Saclay, Orme des Merisiers, 91191 Gif-sur-Yvette Cédex, France

dzitko@discovery.saclay.cea.fr

Helmut Feuchtgruber (FIRST/PACS)

Max-Planck-Institut für Extraterrestrische Physik, Giessenbachstrasse Postfach 1603, Garching, D-85740, Germany

fgb@mpe.mpg.de

Carlos Gabriel (ISOPHOT)

XMM Science Operations Centre, Astrophysics Division, Space Science Department of ESA, Villafranca del Castillo, P.O. Box 50727, 28080-Madrid, Spain

cgabriel@iso.vilspa.esa.es

Pedro Garcia-Lario (ISO Cross-Calibration)

ISO Data Centre, Astrophysics Division, Space Science Department of ESA, Villafranca del Castillo, P.O. Box 50727, 28080-Madrid, Spain

pgarcia@iso.vilspa.esa.es

Ana M. Heras (chair) (SWS glitch statistics/FIRST)

Herschel Science Centre, Astrophysics Division, Space Science Department of ESA, ESTEC, P. O. Box 299, 2200 AG Noordwijk, The Netherlands

aheras@astro.estec.esa.nl

Petteri Nieminen (Space Weather/radiation effects simulations)

Space Environments and Effects Analysis Section, Mathematics & Software Division, ESA, ESTEC, P.O. Box 299, 2200 AG Noordwijk, The Netherlands

Petteri.Nieminen@esa.int

Sunil D. Sidher (Contact person at NDC, LWS)

Rutherford Appleton Laboratory, Chilton, Didcot, Oxfordshire, United Kingdom

S.D.Sidher@qmw.ac.uk

Ekkehard Wieprecht (SWS OLP and IA)

Max-Planck-Institut für Extraterrestrische Physik, Giessenbachstrasse Postfach 1603, Garching, D-85740, Germany

ewieprec@mpe.mpg.de

1.3.3 GWG meetings

The ISO/FIRST Glitches Working Group has had the following meetings:

Meeting #1, held at VILSPA on October 9, 1998 (minutes, viewgraphs)

Meeting #2, held at VILSPA on January 27, 1999 (minutes, viewgraphs)

Meeting #3, held at VILSPA on September 13, 1999 (minutes, viewgraphs)

Meeting #4, held at ESTEC on April 12, 2000 (minutes, viewgraphs)

Meeting #5, held at ESTEC on July 6th, 2000 (minutes)

Meeting #6, held at ESTEC on October 11th, 2000 (minutes)

1.3.4 Participation in conferences

Presentations related to the work of the ISO/FIRST Glitches Working Group have been or will be made in the following workshops/conferences:

ISO Detector Workshop, 14-16 January 1998, ESA-VILSPA, Madrid, Spain; Proceedings published in Experimental Astronomy, vol. 10, Issue 2/3, August 2000.

ESA Workshop on Space Weather, 11-13 November 1998, ESTEC, Noordwijk, The Netherlands; Proceedings published in ESA WPP-155, ISSN 1022-6656, March 1999.

2000 IEEE Nuclear and Space Radiation Effects Conference, 24-28 July 2000,; Proceedings are to be published in the IEEE Transactions on Nuclear Science, December 2000.

The Calibration Legacy of the ISO Mission, 2-5 February 2001; ESA-VILSPA, Madrid, Spain; Proceeding to be published in ESA Special Publications Series (SP-481).

1.3.5 Web pages

The following Web pages gather information on ISO/FIRST Glitches Working Group related activities:

http://isowww.vilspa.esa.es:1909/~pgarcia/glitches.html/ (only for internal access)

http://www.estec.esa.nl/wmwww/wma/ISO/

2. General description of glitches

A particle that hits a photo-conductor detector deposits a certain amount of energy that depends on the type and energy of the particle, the detector material and the length of the particle track in the detector. Glitches were detected and removed from the ISO data following deglitching algorithms implemented in the ISO Off Line Processing. In some cases more sophisticated and/or interactive deglitching methods have been provided in the Interactive Analysis software packages (see section 4). A description of the glitches detected by each instrument follows.

2.1 ISOCAM

A glitch is the result of an energy deposit from charged particles in ISOCAM detectors. This energy deposit is spatially localized (see Figure 2-1) and it takes a limited period of time for the detector to recover from it. A glitch can thus be detected by using spatial and/or temporal criteria. Spatial and temporal properties of glitches depend of the origin of the incident particle. Glitches can be divided into 3 families based on their temporal profile. Temporal families defined for LW detector are given below:

- Type-A, common glitches (see Figure 4 in Claret et al. 1999),
- Type-B, faders where the pixel value decreases slowly until a stabilized value is reached (see Figure 5 in Claret et al. 1999),
- Type-C, dippers where the pixel value decreases first below the stabilized value, and then increases slowly until the stabilized value is reached (see Figure 6 in Claret et al. 1999).

A library containing the most common glitches, as well as other interesting glitches for illustration purpose, was built. This library is accessible to the community (A. Claret and H. Dzitko, ISOCAM Glitch Library, http://www.iso.vilspa.esa.es/users/expl_lib/CAM/glitch_lib/, 1998). Some other families could be considered taking into account the origin of the glitch impact (proton, electron, heavy ion,...). Some glitches display some extensions or a curved shape (see Figure 2-1) depending on the nature and energy of incident particles.

The glitch temporal profile is related to the LET of charged particles interacting with the detectors. The analysis of the temporal profiles leads to the conclusion that Type-A glitches are induced by both trapped and galactic protons and electrons, whereas Type-B glitches are induced by energetic protons, electrons and light galactic ions. Type-C glitches would be induced by particles providing higher LET such as heavy galactic ions.

(*Extracted and adapted from Claret et al. 1999. See this publication, Claret et al. 2000 and Claret & Dzitko 2001a for further information.*)

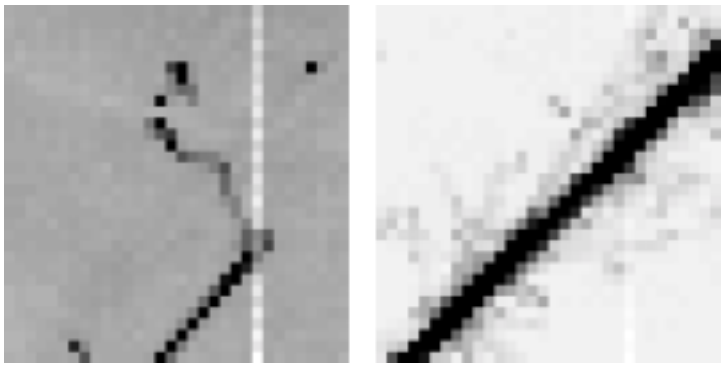

Figure 2-1 Examples of particle impacts on the ISOCAM instrument. On the left panel a low energy particle has probably stopped in the detector, while on the right panel a heavy ion passing through can be seen.

2.2 LWS

There was roughly one glitch per ten seconds per detector during the normal period of LWS operation. These energetic particles caused a sudden jump in the ramp voltage, due to a quantity of charge being dumped on the integrating amplifier. They also caused a change in the detector responsivity which affected the following ramps. “Slow” glitches are glitches where the jump in voltage covers more than one read-out value. In addition to these “positive” glitches, “negative” glitches have also been found. These caused a sudden decrease in the ramp voltage, rather than an increase. They are thought to be due to hits on the FET. Negative glitches did not appear to affect the detector responsivity. *(Extracted from section 3.3.5 of ISO Handbook Volume IV.)*

Figures 4 and 5 of Swinyard et al. (2000) shows the effect of the ionising radiation on an integration ramp and a negative glitch, respectively.

2.3 ISOPHOT

On the ISO orbit all ISOPHOT detectors were continuously affected by the hits of high energy cosmic particles and secondary particles generated by hits into the satellite shielding. This effect constitutes one of the main sources of signal disturbance. The flux of high energy particles depends on the orbital position of the satellite with respect to the radiation belts and the space weather conditions. Every cosmic particle carrying enough energy to produce a band transition is able to cause a sudden jump in the temporal sequence of signals, generally called “glitch”. The main effect of glitches is a degradation of the signal-to-noise ratio, which results in a reduced photometric accuracy.

The continuous hits of high energy particles affect the data in different ways:

1. Decrease of the signal-to-noise ratio: The most common effects of glitches are discontinuities appearing in the integration ramps. This leads to a poorer determination of the signal from the

affected ramps and hence a degradation of the signal-to-noise ratio. Such affected parts of a ramp have to be identified and excluded from the signal determination.

2. Short term variation of the detector response: The disturbance of the integration ramps depends on the relative ratio of the energy deposited by the cosmic particle in the detector to the amount of incoming IR radiation. For a high IR flux level and normal space weather conditions a hit affects only a few readouts, i.e. the relaxation time is relatively short. However, if the charged carrier generated by a cosmic particle is large compared to the photocurrent produced by the IR photons then a hysteresis effect appears. The relaxation time lasts for several integration ramps generating a tail-like signal excess, which is interpreted as a momentary response variation. These glitches are more difficult to identify and to correct for. Severe cases occur if the affected signals constitute an important fraction of the whole signal sequence on a certain sky position, or if the relaxation time becomes as long as the time interval between consecutive glitches.

3. Long term increase of the responsivity: During the pre- flight calibration it was found that the responsivity of the detectors changed after exposing them to high energy radiation. The same behaviour was found in flight, affecting mostly detectors based on Ge:Ga (P3 and C100), whereas those based on Si are less affected (P1, P2 and SS/SL).

4. Increase of the detector “dark signal”: Low energy glitches affect the measurements by increasing the level of the signal measured under zero illumination. The consequence is an increase of the minimum measurable signal, or equivalently, a decrease of the sensitivity limit (see Section 6 in Lemke et al., 1996). The value of the dark signal, including a mean variation along the ISO revolution has been calibrated for each detector/pixel and is available both in the PIA as well as in the Off-line Pipeline Processing (OLP).

(Extracted from Gabriel & Acosta-Pulido 2000. See this publication for further information)

2.4 SWS

Glitches occur within the integrating ramps or during the reset pulse. The resulting change in the slope of the ramp may have positive or negative polarity. As seen after amplification and high-pass filtering they may have any amplitude between telemetry resolution and telemetry saturation. The response to a glitch usually is visible in one or two samples but strong glitches can affect up to 4 samples. Figure 8.5 of the ISO Handbook Volume VI shows an example of a ramp affected by glitches.

After a strong glitch event which pushed the detectors into saturation it can take more than one reset interval to recover. A glitch in an array detector channel affects virtually all detectors in the array by crosstalk. Crosstalk is a capacitive coupling between detector channels happening mainly in the IA12 J-FET arrays. The Fabry-Perot detector channels seem to have no crosstalk. Crosstalk corrections on the non-AC-corrected telemetry level remove a considerable amount of small spike signals from array detector channels. However, the correction can introduce some new spikes reversed in polarity. This is due to the fact that the cross talk matrix has been computed out of a

large number of glitch events, and averaged values have been filled into the calibration file. Thus some glitch events are undercorrected others overcorrected. Negative glitches might be caused by the described overcompensation of the cross correction algorithm or a hit in the electronics. On the other hand a hit on the electronics might introduce fake glitches in the other channels after crosstalk correction.The complexity of these glitch patterns precludes the establishment of a physical model which could be used to recognize glitches and remove their effect.

An additional feature are the so called glitch tails (see example in Figure 8.6 of the ISO Handbook Volume VI). Studies have shown that this detector behaviour contribute significantly to the overall noise, especially for detector band 4 (Ge:Be). Further analysis indicate that tail effects might have an in-reset and long term component. The in-reset effect is increasing the partial slope after a glitch within the same reset interval. This increase in slope is linear correlated with the glitch height and might be up to 40% compared to the undisturbed partial slope.The long term component might last even over a few reset pulses. An explanation might be the changing detector responsivity or change in dark current due to the particle hit. Investigations to characterize the tail effects are ongoing.

(Extracted and adapted from Wieprecht et al. 2000. See this publication for figures and further information).

3. Radiation effects on the ISO detectors

3.1 The space radiation environment during the ISO mission

ISO was launched on 17 November 1995 into a highly elliptical orbit of a 24 hours period, with the perigee and the apogee located at 1000 km and 70,600 km, respectively. ISO finish its operations on 10 May 1998, after the post-helium phase. The space radiation environment in which ISO was operated had four main constituents: the trapped proton belts, the trapped electron belts, the solar protons and the galactic cosmic rays. Around perigee passage the instruments were switched off to avoid radiation damage induced by the proton belts. The instrument activation window was open between 1h 55m and 3h 20m after perigee, when the satellite altitude was around 26500 km. The scientific observations window started 4 hours after perigee passage, at an altitude of 43214 km, and had a duration of 16h 56m with a short interruption of 15 m, for the antenna hand over between the ESA VILSPA and NASA Goldstone ground stations. A description of the trapped protons and trapped electron belts can be found in Evans (1998).

The radiation environment affecting the ISO scientific observations consisted mainly of galactic cosmic rays and electrons from the radiation belts. The galactic cosmic rays are fully stripped atoms composed with 87% protons, 12% alphas, and 1% heavier nuclei. The major part of these particles cannot be stopped by a shield since its differential spectrum is peaked at about 500 MeV. The trapped electrons produce bremsstrahlung in the detector surrounding materials. The maximum energy of the γ-rays produced is about 3 MeV and the mean energy ~ 0.5 MeV. The bremsstrahlung may in turn give rise to secondary electrons which can hit the detectors.

Since the ISO mission was carried out during solar minimum, the solar energetic particle contribution was not significant. Figure 3-1 shows this quiet proton flux conditions, just perturbed by a soft event in April 1996 (revolution 152) and by the only energetic event on 4-6 November 1997 (revolution 720-722), during which the proton flux for $E < 10$ MeV and $E < 100$ MeV increased by almost three orders and an order of magnitude, respectively, with respect to its average value. The effects of this solar event on the ISO instruments is given below in section 3.5.2. Additionally, during the post-mission technology test campaign, a moderate solar proton event occurred on 20-23 April 1998, the effects of which were seen as an increased false count rate in the ISO Star Tracker.

The effects of the radiation environment on the ISO spacecraft are described in detail in Evans (1998). The conclusions of this work are: “The ISO mission commenced during a period of solar minimum activity. Little variation in the energetic proton component was expected during this time, and so few anomalous effects to the spacecraft were expected. Ultimately, the proton radiation environment during the mission has been benign, with the exception of the November ‘97 solar proton event and the April ‘96 geomagnetic disturbance. Neither of these events contributed significantly to the overall degradation of the satellite. The April ‘96 event was not severe enough to cause any noticeable effects to the spacecraft. The November event, though, was harsh enough to dramatically increase the background in the star trackers and payload. Although the event’s effect on the long term degradation of solar cells and components is small in comparison to that of the constant radiation belt traversals.”

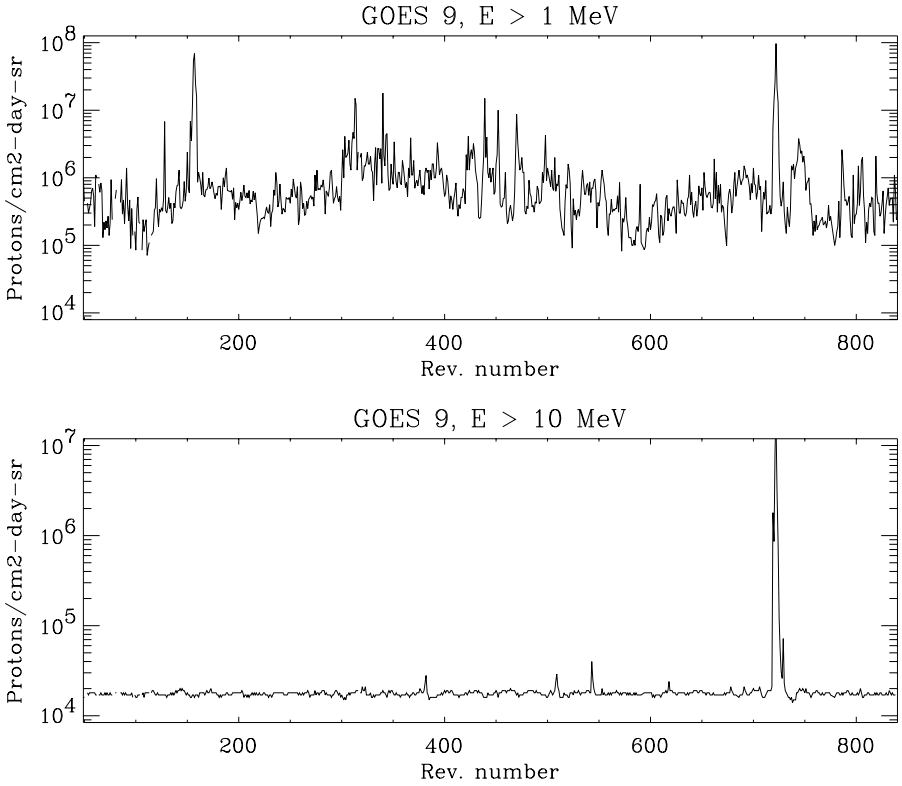

Figure 3-1 Daily proton fluence measured by the GOES 9 satellite (Space Environment Center, NOAA) during the ISO mission.

3.2 ISO shielding

A ray-tracing analysis on the amount of Aluminium equivalent shielding surrounding each of the four ISO detectors was performed in the design phase of the mission and is described by Moret-Bailly and Juillet (1989). The information on the Aluminium-equivalent shielding surrounding each of the ISO instruments over 4π was available in the form of a coded data matrix. This was scanned, converted into numerical form, and is plotted in the colour diagrams shown in Figure 3-2. The scale of the diagram ranges from zero to nine cm Al shielding thickness, and shows that the minimum shielding thickness for any of the detectors in any viewing direction is 9 mm. A clear limitation of these data was that any thickness above 13.0 mm was always marked as equal to 13.0 mm. This was presumably due to the original assumption that such shielding information would only be useful with regard to particle populations in the radiation belts. In the belts the proton fluxes are, indeed, much higher and generally more likely to increase the total ionising dose than those of the galactic cosmic rays are. However, these protons are of relatively low energy (up to ~200-300 MeV) and for the glitch phenomena discussed in this document, it is specifically the high-energy cosmic rays, encountered during the science windows that are of importance.

It is recommendable for future infrared missions, notably for FIRST (Herschel), that similar shielding data be calculated in the sensitive detector locations, but without any thickness limits

such as in the ISO shielding data matrix. Ideally, however, for accurate Monte Carlo analysis the best solution is to construct a geometrical model representing the detector and spacecraft structure in which the particles can be transported. For this purpose, it is vital that material, geometry and dimensional information at all levels of the spacecraft are maintained in computer-readable form.

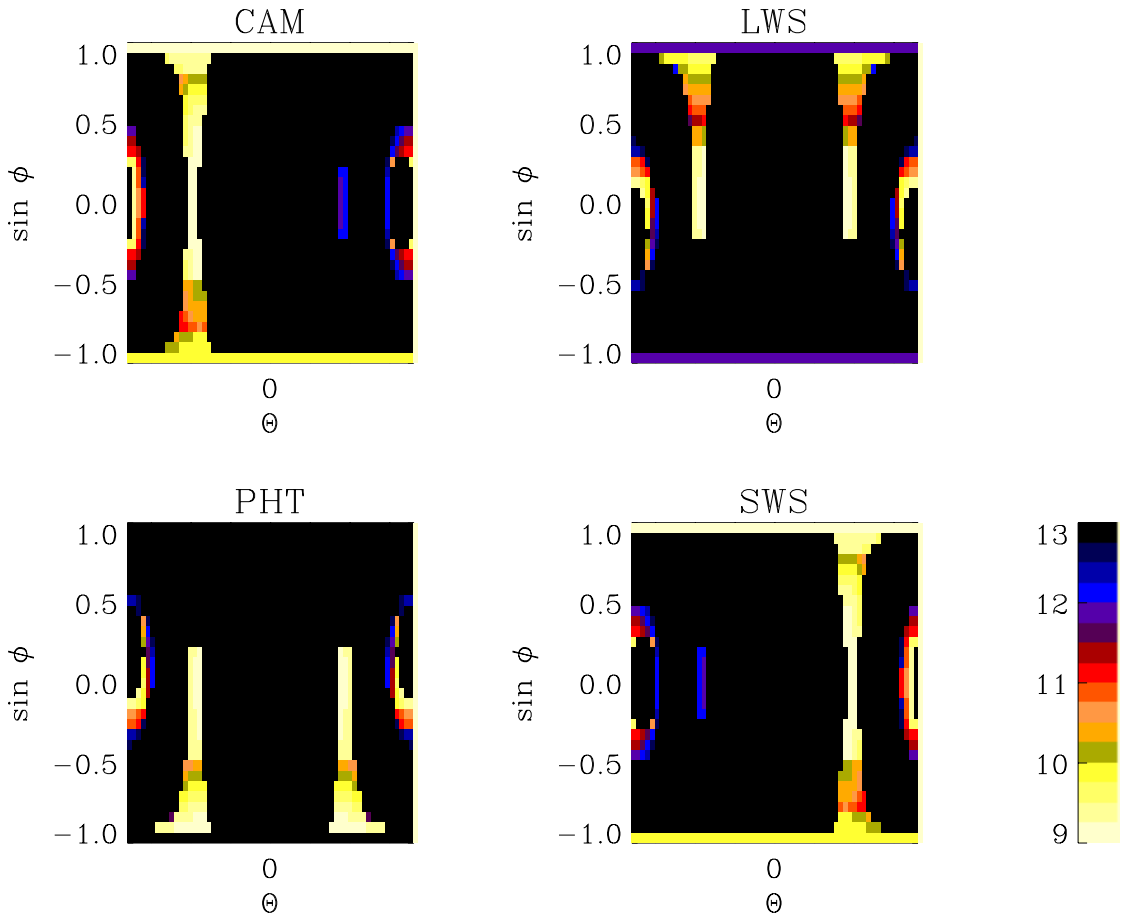

Figure 3-2 Omnidirectional shielding data at the locations of the four ISO detectors. The colour coding indicates Aluminium-equivalent shielding thickness in mm.

3.3 Glitch statistics

3.3.1 ISOCAM

Before the ISO launch, extensive radiation tests were performed on the ISOCAM infrared detector array (Agnese et al. 1991). Low and high dose rate tests were performed with ^{137}Cs sources. The total dose expected to be seen during the mission was about 1.5 krad. From these tests, the conversion factor for γ-rays was estimated to be ~ 0.3 mV/keV. Tests performed with 200 MeV protons lead to a conversion factor of 0.15 mV/keV showing that the glitch amplitude is not line-

arly related to the energy lost by the incoming particles. Tests with Ar beam of 70 MeV/nucleon were made to investigate the behavior of LW detector in presence of high LET particles.

In orbit, the actual glitch statistics from in-flight measurements were:

- Average glitch rate = 1 glitch/sec (for observations with 6 arcsec/pixel lens, see Table 3-7:),
- Average number of hit pixels = 8 pixels/glitch.

These numbers are mean values and correspond to what should be observed during a standard ISOCAM observation. The glitch occurrence follows Poisson statistics but depends also on the space weather. The glitch rate and/or number of hit pixels are of course orbital position and solar activity dependent (see Figures 7 and 8 in Claret et al. 1999). These numbers have been derived from algorithms, which are used to remove glitch effects in ISOCAM data. These algorithms detect a glitch as a different temporal profile or/and spatial pattern than the expected signal (astronomical background + source + dark current + memory effect). This implies that they do not detect glitches separately (2 or more glitches can be considered as a single one, and also several high value pixels can be considered as many different glitches whereas they belong to the same one). Thus, these algorithms can not be used to derive properties of individual glitches, such as the actual duration, number of hit pixels, rising time, and so on. Nevertheless, some effects can compensate each other and the above numbers can be considered as representative.

The effect of glitches are not so dramatic for SW as for LW. This is because the active zone of the pixel is very thin, < 10 μm, so that its volume is very small. Due to the very low energy needed to create a free carrier pair, the charge generation is equivalent for both SW and LW detectors, but the pixel geometry of the SW array ensures that most of the particles cross only one pixel. After a hit the responsivity of the pixel decays slowly to its previous value. The decay time is the same as for transients due to IR flux changes. The lower the illumination of the array, the longer the decay time.

3.3.1.1 Sensitivity Loss

Considering only the number of masked pixels, a rule of thumb is 2% loss for 2.1 sec images, 5% loss for 5.04 sec images, 10% loss for 10.08 sec images. For 20 sec images, it appears that it is very difficult to deglitch data due to the high number of glitches per image. It was advised to ISOCAM observers to avoid using 20 sec integration time. For 0.28 sec images, one could expect less than 1 glitch per image, but since 4 images are co-added on board before being downlinked, there is around 1 glitch per image, corresponding to a sensitivity loss of 1%.

The actual sensitivity loss is higher than the above values due to glitch tails, gain variation, cosmic particles. It is very difficult to assess the global sensitivity loss due to glitches, especially if one considers the robustness of algorithms for faint source detection.

(*Extracted and adapted from Claret et al. 1999. See this publication and Claret et al. 2000 for further information.*)

3.3.2 LWS

The glitch statistics of each observations are given in the OLP generated file LWGHXXXXXXXX, where XXXXXXXX is the TDT number. It contains information about the time at which the glitches occurred, the affected detector and the glitch height (see chapter 6.2.5.3 of the ISO Handbook Volume IV). Some basic properties of the frequency and characteristics of the glitches are described in Swinyard et al. (2000). We shall concentrate therefore in the following on the deposited energy distribution of the observed glitches. The LWS works with integrating amplifiers, and a hit of a detector by an ionising particle leads to a sudden jump in the output voltage. As this jump sits on top of the integration ramp measuring the signal from the source, one might naively assume that large glitches can only be detected in observations of weak sources, where the photocurrent does not come close to saturation of the detectors. This is, however, the opposite of what is observed: Among randomly selected observations of weak and strong sources with similar duration we found only 4 glitches higher than 3 mV for the weak sources compared to 200 such glitches for the strong sources. The reason for this discrepancy is probably the analogue amplifier gain which is set to a higher value for observations of weaker sources and therefore drives bigger glitches beyond the limit with which the cold electronics can cope. Hence we used only long lasting grating observations of strong sources to derive the following pulse height spectra for the LWS detectors*. The glitch height energy distributions given in Table 3-1:, Table 3-2:, and Table 3-3: are represented graphically and compared to other instruments in Figure 3-3 and to the simulations in Figure 3-5. The following conclusions can be drawn from these glitch height distributions:

1. All detector materials show the same glitch rate at the low and high energy end of the histogram. This was expected, because all LWS detectors have Ge as bulk material.

2. The slope of glitch rate = f (Energy) at low energies is steepest for the stressed detectors. This may be due to the fact that for these detectors the photocurrent was closer to saturation than for the unstressed detectors.

3. The discrepancy between observation and model that was reported in Heras et al. (1999) has been greatly reduced by using only observations of strong sources. The remaining difference can be caused by uncertainties in the conversion mV <--> MeV which would change the particle energies calculated from the glitch height** or by remaining systematic effects like underestimation of the strength of glitches which drove even in the observations considered here the detectors into saturation.

* TDT ## 29001726, 32600114, 32600211, 32600310, 32600409 and 46401027; these observations correspond to revolutions without anomalies of the space weather.

** using the formula $E = C * V / e / g * E_g$, where:

E = Energy deposited by ionising particle
C = Input capacitance of amplifier = 7.5E-12 F
V = Voltage jump caused by glitch

Table 3-1: Ge:Be

Energy [keV]	Glitch rate (s^{-1})	Poisson error in Glitch rate (s^{-1})
0-100	0.05428	0.00104
100-200	0.01153	0.00048
200-300	0.00658	0.00036
300-400	0.00235	0.00022
400-500	0.0014	0.00017
500-600	0.0004	0.00009
600-700	0.00034	0.00008
700-800	0.00014	0.00005
800-900	0.0002	0.00006
900-1000	0.00016	0.00006

Table 3-2: Ge:Ga

Energy [keV]	Glitch rate (s^{-1})	Poisson error in Glitch rate (s^{-1})
0-100	0.05243	0.00102
100-200	0.01673	0.00057
200-300	0.00481	0.00030
300-400	0.00172	0.00017
400-500	0.00092	0.00013
500-600	0.00048	0.00009
600-700	0.00029	0.00007
700-800	0.00019	0.00006
800-900	0.00018	0.00006
900-1000	0.00016	0.00006

Table 3-3: Ge:Ga (stressed)

Energy [keV]	Glitch rate (s^{-1})	Poisson error in Glitch rate (s^{-1})
0-100	0.05359	0.00103
100-200	0.00396	0.00027
200-300	0.00089	0.00013
300-400	0.00107	0.00013
400-500	0.00041	0.00008
500-600	0.00025	0.00007
600-700	0.00018	0.00006
700-800	0.00020	0.00006
800-900	0.00016	0.00006
900-1000	0.00017	0.00006

e = charge of electron = 1.6E-19 C
g = photoconductive gain
E_g = band gap in Germanium = 2.9 eV

(See also Burgdorf et al. 2001.)

3.3.3 ISOPHOT

In order to make glitch statistical studies more comfortable, a set of special routines were written, which enable detailed information about glitch detection to be stored in as many data sets as required. For each detection the following information is kept:

- the universal time, permitting long term studies,
- the satellite revolution number, for relating glitch rates changes e.g. to solar activity,
- orbital position (distance to the Earth radiation belts),
- glitch strength,
- mean detector signal.

Additional data can be analysed and easily merged into the existing database. These routines, together with selection and analysis tools, constitute a special package within the PIA environment. The results of glitch statistics have to be taken in so far carefully, since they are very dependent on the success to detect low level glitches, which in turn depends on several factors as the criterion (number of sigmas) to identify glitch events or the detector readout noise. We have determined the glitch rate for the different detectors using observations of same type repeated over the full mission (medium flux level and central orbital position) and results are presented in Table 3-6:. Glitches are detected in the ISOPHOT data with a frequency of one event every 5 to 20 s. The frequency depends on the space weather and the orbital position. Another important issue is the energy deposition spectrum, derived from the glitch amplitude (i.e. the measured voltage difference). The spectra for the ISOPHOT long wavelength detectors C100, C200 and PHT-S is shown in Figure 3-3. The spectral differences between C100/P3 and C200 on the other side are remarkable. One of the reasons for the shift in the spectrum is the smaller bias applied to C200, which cause a different conversion factor between cosmic particle energy deposition and photocurrent achieved. The larger readout noise level of P3 is reflected in a higher cutoff value for the recognition of glitches. In particular data from the C200 detector are being used for detailed studies of cosmic radiation effects (Eckardt 1999) for an optimized design of an instrument on board the satellite FIRST (Herschel).

(Extracted and adapted from Gabriel & Acosta-Pulido 2000. See this publication for figures and further information).

3.3.4 SWS

The statistical study of the glitches in the SWS detectors is based on glitches as identified by the SWS Off-Line Processing V4.5 algorithms (Wieprecht et al. 2000). The detectability of a glitch depends on the slope of the ramp where it occurs. The glitch height in ramps with pronounced slopes must be greater than in flat ramps in order to be detectable. In the same way, the gain setting influences the glitch recognition. Applying a certain gain to a ramp results in multiplying the glitch height by the corresponding gain factor. This amplification ensures that a glitch that would be confused with the ramp noise, stands out after applying a higher gain. As a consequence, observations with low gain have associated lower glitch rates. For consistency, we have restricted our study to observations in which the gain was set to the maximum value, 16x. In absolute terms, the instrument design, the noise of the ramp measurement and the glitch recognition software set the minimum and maximum glitch height that can be detected (see Table 3-4:).

Table 3-4: Minimum and maximum voltage jumps detectable in SWS glitches

Gain	Minimum voltage (mV)	Maximum voltage (mV)
Gain 1x	0.1	88
Gain 4x	0.027	22
Gain 16x	0.007	5

From the comparison of glitch rates in observations taken at different times during a revolution, it can be clearly seen that glitch rates in measurements taken close to perigee (in the end of the activation window) are in all cases higher than in observations executed close to apogee. This shows the influence of the electron radiation belt in the particle hits on the detectors before the start of the science observation window. More details on the calculations and to see the corresponding figures can be found in Heras et al. (2000). For the astronomical observations, that is, performed in the observations window, no trend of the glitch rates in any of the SWS detector bands was observed.

Table 3-5: displays the average glitch rates for each SWS detector band, calculated from all measurements with gain 16x. The third column shows the glitch rate per detector unit area, in which the detector average projected area has been taken as (lw + lh + wh)/2, where l, w, and h are the dimensions of the detector. As can be seen, the most affected detectors are the Ge:Be ones, with glitch rates almost one order of magnitude higher than in the other bands. In bands 1 and 3 the determination of the glitch rate per unit area is difficult due to the very small z-dimensions of the detectors, which are not precisely known.

There are three main factors that influence our glitch rate calculation. First, the first six samples in a ramp are discarded in the data processing to avoid the after-reset-pulse effect. Taking this fact into account would increase the derived glitch rates by ≈ 15%, depending on the reset time interval. Second, due to residual cross-talk in the detector arrays, one particle hit may be counted as several glitches, an effect that is particularly significant in band 6 (Ge:Be). A glitch temporal analysis in this band shows that the calculated glitch rate is overestimated with respect to particle hits

Table 3-5: Glitch rates in SWS detectors

Detector band	Glitch rate (gain 16x) (s^{-1})	Dimensions (mm)	Glitch rate (cm^{-2} s^{-1})
Band 1, InSb	0.005 +/- 0.002	0.12 x 0.12 x ≈0.001	-
Band 2, Si:Ga	0.025 +/- 0.005	0.12 x 0.12 x 2	10.0
Band 3, Si:As	0.015 +/- 0.007	0.42 x 0.37 x ≈ 0.001	19
Band 4, Ge:Be	0.18 +/- 0.05	0.45 x 0.45 x 2	17.8
Band 5, Si:Sb	0.09 +/- 0.02	0.165 x 0.675 x 2	10.1
Band 6, Ge:Be	0.11 +/- 0.03	0.3 x 0.7 X 2	10.1

by 25%. The third factor that may influence the glitch counts are the saturating glitches, which for SWS were not included in the OLP glitch tables used in the analysis. As shown in the technical note Report on the effect of saturating glitches on SWS glitch data, the estimated percentage of saturating glitches not included in the values of Table 3-5: is 3% for the Si:Ga band and 9% for the Ge:Be band. The nett result from the effect of these three factors in band 6, where they are most important, is that they compensate each other. Therefore we can conclude that the value displayed in Table 3-5: is rather accurate.

An important result is that the glitch rates per unit area (third column) are between 2 and 4 times higher than the value of 4 particles (cm^{-2} s^{-1}) for the cosmic ray flux, predicted by the CREME96 model (Tylka et al. 1997; Nieminen & Sörensen 2000). This indicates that in addition to the cosmic rays, the glitch rates in the SWS detectors are the result of another type of particle impacts. In section 3.4 it will be shown that these particles are δ–rays and other secondary particles produced by the proton and electron flux in the detectors and the shield.

The glitch height is directly related to the energy deposited by the particles that hit the detector. Knowing the detector material characteristics, it is possible to derive information about the incident particles. Moreover, the glitch distributions as a function of deposited energy provide a good basis for the comparison among ISO instruments and with the results from the models. The deposited energy by a particle hit has been calculated from the corresponding voltage jump height, V, following the expression:

$$E = C * V / e * E_g$$

where C is the input capacitance of amplifier ($7.5\ 10^{-12}$ F), e is the charge of the electron and E_g is the energy loss per electron-hole pair produced, which is 3.6 eV in Si and 2.9 eV in Ge. The resulting energy deposited distributions for detector bands 2 and 4 can be seen in Figure 3-3 and Figure 3-4. In section 3.2.3 of Heras et al. (2000), a more detailed description on the glitch height analysis can be found. Figure 12 of the same work shows the energy deposited distributions for the different types of observations analysed. Although the energy deposited distributions for observations performed closer to perigee and apogee were almost identical, a higher number of

low energy impacts was seen closer to perigee, probably in association with the higher electron flux.

3.3.5 Comparison between instruments

Table 3-6: displays the glitch rates per unit area for the different ISO instruments sub-systems. The results show that when comparing values for the same detector material, the observed glitch rates agree within a factor of 2-3.

Table 3-6: Comparison of observed glitch rates in the ISO instruments

Detector type/ Instrument	Glitch rate (cm^{-2} s^{-1})	Minimum E deposited (keV)
Si:Ga		
CAM	14.9	-
PHT-P1	6.5	1
PHT-S	5.8	1
SWS	10.0	1
Ge:Be		
LWS	6.3	1.9
SWS	17.8	0.95
SWS-FP	10.1	0.95
Ge:Ga		
PHT-P3	10.1	1
PHT-C100	12.5	1
LWS	7.0	1.2
PHT-C200 (stressed)	7.3	1
LWS (stressed)	6.7	1.3

A comparison of the glitch height distributions (or energy deposited distributions) for different ISO instruments is given in Figure 3-3. The result of the comparison shows:

- ISOPHOT-S and SWS glitch rates in Si:Ga detectors show a good agreement. ISOPHOT-P1 detected less small glitches and more energetic hits than these detectors.

- For the Ge:Ga detectors, the LWS and the ISOPHOT-C200 energy deposited distributions are very similar, especially at higher deposited energies. The ISOPHOT-C100 energy deposited distribution is similar to the ISOPHOT-P3 one, both being above LWS and ISOPHOT-C200. As mentioned before, one of the reasons for the shift in the spectrum is the smaller bias applied to C200, which causes a different conversion factor between cosmic particle energy

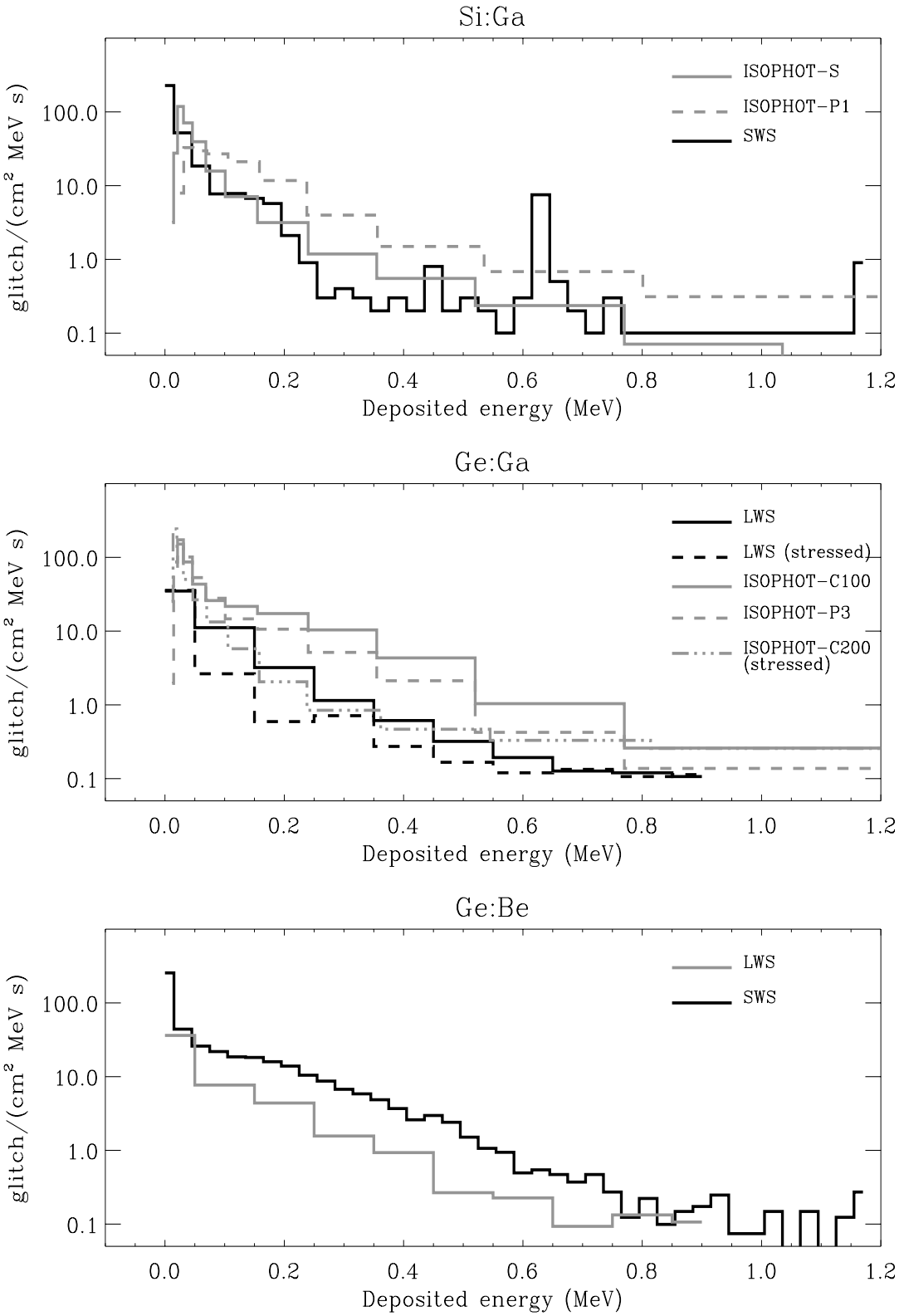

Figure 3-3 Comparison between instruments of the glitches energy deposited distributions for three detector materials.

deposition and photocurrent achieved. The larger readout noise level of P3 is reflected in a higher cutoff value for the recognition of glitches.

- In the Ge:Ga detectors, the slope the glitch height distribution is steeper for the stressed detectors, both in ISOPHOT and LWS. In LWS the reason may be that these detectors the photocurrent was closer to saturation than for the unstressed detectors.

- For the Ge:Be detectors the energy deposited distribution is higher in SWS than in LWS. The slope of the distributions is similar, although it can be seen that SWS detected a larger fraction of small glitches.

- A comparison between the results from Ge:Ga and Ge:Be shows that the SWS distribution agrees with the ISOPHOT-C100 and the ISOPHOT-P3 ones.

- The energy deposited distributions in the Si detectors are steeper than the distributions in the Ge detectors.

- All the energy deposited distributions peak at the lowest detected energies.

Considering the diversity of instrument designs, instrumental data and software used, we conclude that the glitch rates and energy deposited distributions observed by the ISO instruments are consistent. The differences found can be explained by the following factors:

(i) the instrument shielding;

(ii) cross-talk between detectors;

(iii) the efficiency of the algorithms in the detection of small glitches, which is particularly important because they are the most numerous;

(iv) the uncertainty in the values of the photoconductive gain (especially for LWS), which affects the conversion from voltage jumps to energy deposited in the detectors;

(v) the number of undetected glitches due to saturation.

3.4 Simulation of radiation effects on the ISO detectors

3.4.1 Monte-Carlo simulations of the ISO instruments glitch effects

Two main approaches were used in simulating the glitch effects on the four ISO detectors, both utilising the CERN-originated Geant3.21 Monte Carlo particle transport package (*GEANT, Detector description and Simulation Tool*, 1994). The first one was based on ray-tracing techniques, whereby non-interacting rays were isotropically aimed at the target detector and the resulting distribution of track lengths within the detector volume was registered. These distributions were consequently converted into energy deposits in the detector material assuming the incident particles

were Minimum Ionising Particles (MIP). Due to the absence of physics treatment, this method has to be considered approximated only, but in an environment dominated by high-energy MIP cosmic rays that can penetrate a very thick shielding it provides a reasonable first approach and does not require excessive computing time. The radiation environment in the ISO science windows, i.e. outside the radiation belts, was clearly dominated by such cosmic rays since the mission took place during a solar minimum. Figure 3-4 shows the comparison between the model results and

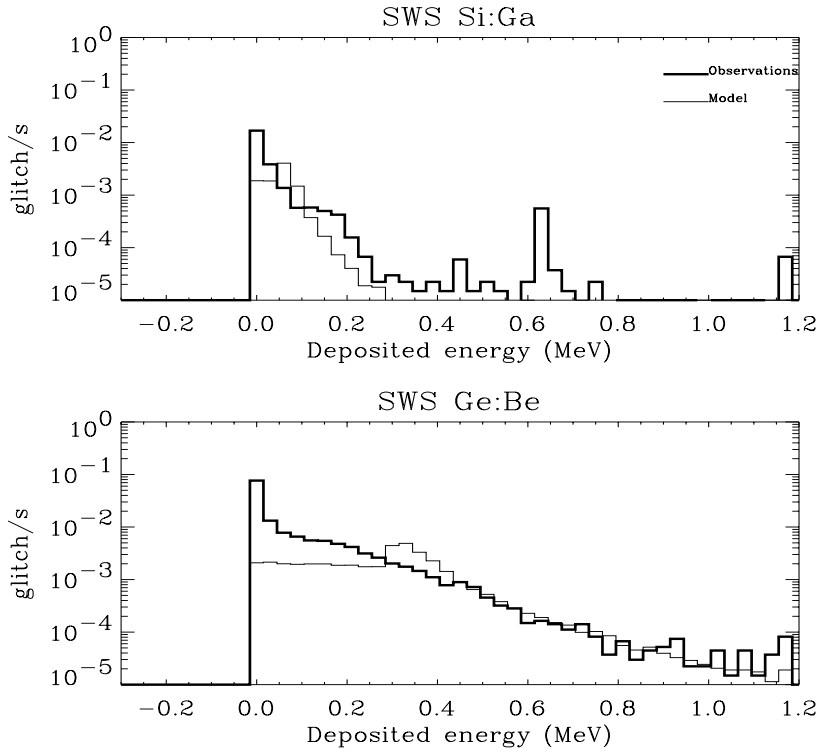

Figure 3-4 Deposited energy distribution of the observed glitches in the SWS instrument and the results from a ray-tracing simulation.

the observations for the glitch height distributions in two types of SWS detectors, after the simulation data have been normalized to the corresponding SWS observed glitch rates. The simulations reproduce well the glitch distribution for high energy impacts, but the predicted glitch rate is underestimated for the lower deposited energies, especially in the Ge:Be detectors. The origin of the lower energy glitches can be understood by considering that the average energy deposited by a secondary electron, emitted on absorption of a Bremsstrahlung photon produced after the absorption in the satellite material of a trapped electron, is 01-0.2 MeV in Si and approximately 0.1 MeV in Ge. Since ray-tracing simulations assume non-interacting rays, the discrepancy between the observations and the model can be explained by the non inclusion in the simulations of δ–rays (secondary electrons of a target material which are ejected along the track of an incoming particle) and other secondary particles produced by protons and electrons in the detectors and the shield.

The other method, used here only in the case of the LWS detector, also used isotropic fluxes but employed a full simulation of the physical processes occurring along the track of the incident particles and their secondary particles, also taking into account the local shielding. This approach was used for LWS due to the disagreement between the ray-tracing analysis results and the experimental glitch data from that detector (for the other three instruments, the ray-tracing method provided a fair agreement with on-flight data, see Figure 3-4). However, even the full physics treatment is not sufficient to completely bridge the gap between the simulated and experimental LWS energy deposit distributions. In Figure 3-5 the integral spectrum derived from the Monte-Carlo simulations is plotted with the observational LWS data. The ISOPHOT data is also shown, since the simulations are also applicable to detectors of the same size and material as the LWS's (ISOPHOT-C200 and ISOPHOT-P3). Figure 3-5 shows that the model underestimates the LWS glitch rates for the low deposited energies (< 0.1 MeV) and overestimates the glitch rates at higher deposited energies. The model reproduces better the ISOPHOT-P3 and ISOPHOT-C100 distributions at energies greater than ~ 0.2 MeV, but the discrepancy at lower energies is still important. The Monte-Carlo simulations include the effects of the incident cosmic rays as well as the production of δ-rays and secondaries in the detectors and the shield. However they do not consider the effect of the incident electron flux, which has been associated with variations in the glitch rate and in the performance of the detectors (see section 3.5.1). With the minimum shielding of 9 mm Aluminium equivalent, electrons in the outer radiation belt need energies of at least 4 MeV to reach any of the ISO detectors. These electrons produce γ-rays by bremsstrahlung in the detector surrounding materials, which may in turn give rise to secondary electrons which can hit the detectors. Eckardt (1999) estimated that the resulting integrated spectrum of hits due to electrons was ~ 50% of the integrated spectrum due to protons, for energies lower than 0.1 MeV. Therefore including the electron contribution in the Monte-Carlo simulation shown in Figure 3-5, would significantly improve the consistency between model and observations at low energies.

More detailed accounts of the LWS simulations, together with supporting analytical calculations are given in Simulations of radiation effects on the ISO detectors (P. Nieminen).

For studies of this type, the standard tool used by ESA today is the Object-Oriented Geant4 particle transport toolkit (Apostolakis et al. 2001). With its Sector Shielding Analysis Tool (Truscott et al. 2001), low-energy electromagnetic physics extensions (Chauvie et al. 2001) and wide selection of other options and tools, this provides the capability for highly detailed engineering analyses.

3.4.2 Predicted glitch rates for ISOCAM

Along the ISO orbit, the perturbations come from cosmic rays and trapped particles in the van Allen belts. Their fluxes are defined within a factor 2, depending on the solar activity. Primary particles passing through the surrounding materials also produce about 50% of additional events either by nuclear reactions or δ-ray emissions. Latest predictions can be summarized as follows:

- 0.36 s^{-1} of direct impacts from cosmic rays,
- 0.29 s^{-1} of secondary particles and δ-rays from materials near the detector and activated by cosmic particles (contribution is ~80% of direct impacts),

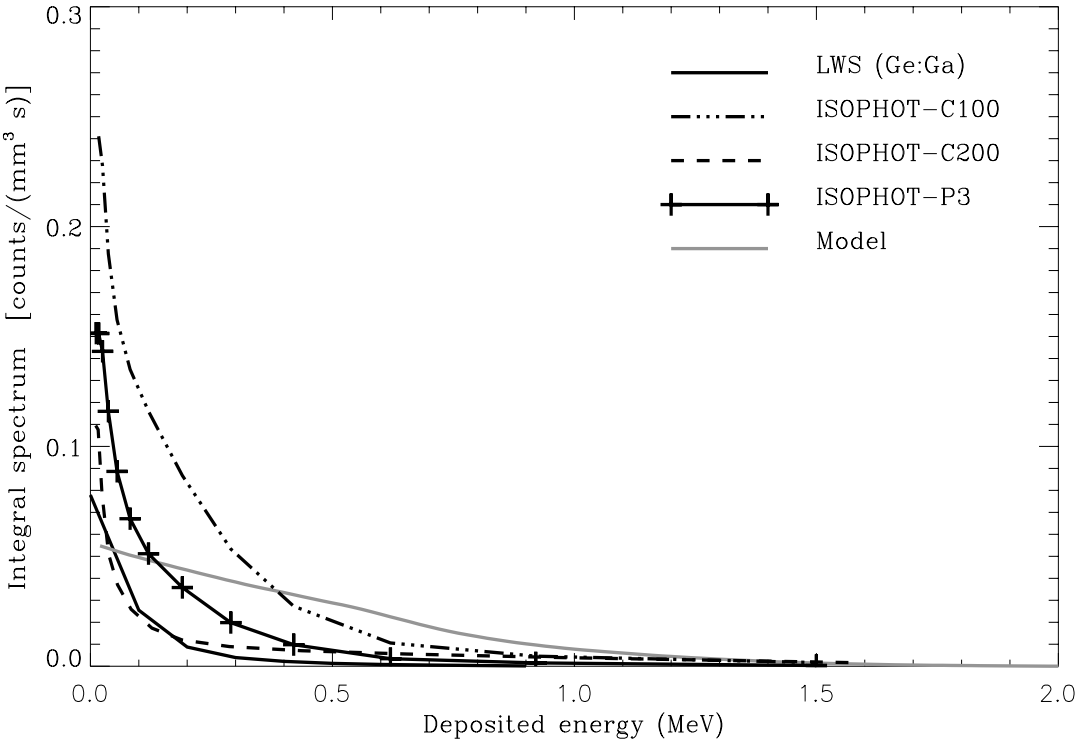

Figure 3-5 Integral spectrum the glitch energy deposited distributions and the comparison with the model.

- Additional contribution from activated materials in the body of spacecraft.

The previous estimation of direct impacts was a bit less than this one (0.28 s^{-1} instead of 0.36 s^{-1}). This is due to a different estimation of the number of trapped particles. In this paper, the number of direct impacts is based on new measurements by the KET 3 on board of the Ulysses spacecraft (Oct-1997 and Feb-1998, when it was close to the ecliptic plane). In addition to these external particles, the anti-reflection coating of lenses contains ^{232}Th, which generates a flux of low energy α-particles. The α-particle flux depends on the solid angle of the lens viewed from the array, and is maximum for the 12 arcsec/pixel lens:

- 0.35 s^{-1} from the 12 arcsec/pixel lens,
- 0.16 s^{-1} from the 6 arcsec/pixel lens,
- 0.02 s^{-1} from the 3 arcsec/pixel lens,
- 2 10^{-3} s^{-1} from the 1.5 arcsec/pixel lens.

Neither the electro-magnetic showers, nor the secondary particles from the body of spacecraft have been taken into account here. These last contributions are more difficult to derive and require Monte-Carlo simulations. It is very likely that a few tenths of glitch/sec might be added. Based on the above numbers, the latest estimation of glitch rate is given in Table 3-7:. Since uncertainties about the contributions of secondary particles and δ-rays still remain, these results should be taken only as orders of magnitude, and at least as lower limits.

Table 3-7: Predicted glitch rates (s^{-1})

Contribution	1.5” lens	3” lens	6” lens	12” lens
Primary GCRs	0.36	0.36	0.36	0.36
Secondary particles and δ-rays	0.29	0.29	0.29	0.29
α-particles produced by ^{232}Th	0.002	0.02	0.16	0.35
TOTAL	**0.65**	**0.67**	**0.81**	**1.0**

See Dzitko et al. (2000) for a detailed description and discussion on the calculations of the predicted ISOCAM LW glitch rates.

(*Extracted and adapted from Claret et al. 1999. See this publication or Claret et al. 2000 for further information.*)

A Monte-Carlo simulation tool was built for ISOCAM. It was calibrated on in-flight data. Some results about the deposited energy by incoming particles are presented in Figure 5 of Claret and Dzitko (2001a). Note that the electronic response of the detector was not simulated. A detailed paper about these simulations is in preparation (Claret and Dzitko 2001b). It is possible to use this tool in order to simulate radiation effects for future space experiments, such as the NGST or the bolometer detectors of FIRST/PACS. *(Extracted from Claret and Dzitko 2001a.)*

3.5 Correlation between glitches and space weather

3.5.1 Correlation between glitch rates and electron fluxes

A thorough study of the temporal evolution of glitch rates was carried out for the SWS. The selected observations were: (1) Observations in calibration revolutions (once a week) just after the science window started; (2) observations in calibration revolutions executed around apogee passage; (3) daily measurements at the end of the activation sequence (3 hours after perigee passage); and (4) daily observations at apogee. In Figures 9 and 10 of Heras et al. (2000), the glitch rates for SWS bands 2, 4, 5 and 6 are plotted as a function of ISO revolution number and are compared to the electron fluxes with E > 0.6 MeV and E > 2 MeV measured by GOES 9. These Figures show a clear correlation, both in the long and short term features, between the glitch rates in bands 4, 5, and 6 and the electron flux, for the observations carried out close to perigee (when ISO and GOES 9 were at similar altitudes, 4.5 R_E). In the other bands, the calculated glitch rates were not high

enough for the correlation to appear clearly, because of the smaller detector areas. No correlation with the GOES 9 electron flux measurements is seen for observations executed around apogee passage, probably due to the different electron environment in that region (unfortunately we do not have electron flux measurements there). We can therefore conclude that the SWS Ge:Be and the Si:Sb detectors are rather sensitive to electron impacts, which is clearly seen when the satellite crosses the electron belts in high flux regions. In addition to the electron flux contribution, the glitch rate modulation seen in SWS bands 4, 5 and 6 may be also related to the position of the ISO orbit with respect to the magnetosphere. Particularly, in revolutions 215 and 645, when the glitch rates show lower values, the orbit apogee was located at 180 degrees from the Sun-Earth line. In revolution 430, on the contrary, the ISO apogee was located between the Sun and the Earth on the Sun-Earth line, such that the satellite might have been out of the magnetosphere and therefore more vulnerable to solar particles.

The LWS detectors (Ge) were also especially affected by particle impacts around the start and end of the science observation window, at altitudes lower than 43000 km. Above this altitude the glitch rate decreased by a factor of two abruptly, keeping to a constant level afterwards, a behaviour that seems to be related to the structure of the electron belts.

In ISOCAM, just before or after the end of scientific window, glitches induced by electrons were more numerous and the glitch distribution was slightly different than the standard one (see Figure 7 in Claret et al. 1999).

These glitch rate correlations with the electron flux add another argument to support that a large fraction of the impacts detected were associated secondary particles produced in the detector and the shield.

3.5.2 Effects on the detectors of the 6 November 1997 large proton event

The solar proton event on 6 November 1997 was the only intense event to have occurred during the ISO mission. The proton flux was almost three orders of magnitude higher than average for protons with E > 10 MeV, and more than one order of magnitude higher for protons with E > 100 MeV. A more detailed description of the event can be found in section 3.2.2 of Heras et al. (2000). The dark currents, dark current noise and glitch rates in all instruments increased so dramatically that most observational data was corrupted and all observations in revolution 722 were declared failed. All parameters were back to normal values in the following revolution, except for LWS, in which the dark currents and responses were still higher than nominal.

In the ISOCAM data the effect of the solar flare was striking. The glitch rate increased by a factor between 7 and 10 (see Figure 8 of Claret et al. 2000). For the first time during the mission all six ISOPHOT detector systems showed signals out of their nominal range. The impact on the data lasted for the full revolution, and, beside the high responsivity, all the measurements were so severely affected by the high rate of glitches that they had to be declared failed.

Concerning SWS, the most affected observation was the first one in the revolution, at the time the proton flux was at its maximum. Figure 11 of Heras et al. (2000) shows the detector behaviour in revolution 722. The dark current noise increased by 200% in all bands. The dark current level

increased by 200% in bands 1 and 4, 25% in band 3, an it remain stable in band 2. The responsivity (dark current subtracted) actually decreased during the proton event, by 30%, 10% and 15% in bands 2,3, and 4, respectively. The glitch rate reached values between five and ten times the nominal rate in all bands, decreasing after its maximum during the first observation. The deposited energy distribution of the particle impacts during the proton event was harder than average, that is, more high energy impacts were registered as a result of the increased flux of high energy protons (Figure 12 of Heras et al. 2000).

All detector parameters were back to normal in the following revolution, although the flux of protons with E >10 MeV had only decreased by half an order of magnitude. Possible reasons are that the detector behaviour was only affected by high fluxes (> 100 protons/cm^2-s-sr) of protons with E > 30 MeV, or mainly by the higher energy protons (E > 100 MeV). This is consistent with the fact that low energy protons could not penetrate the shield, as expected from the shielding model for ISO. It may also indicate that the contribution to the glitch rate from electron injection events taking place during the intense geomagnetic disturbances was significant.

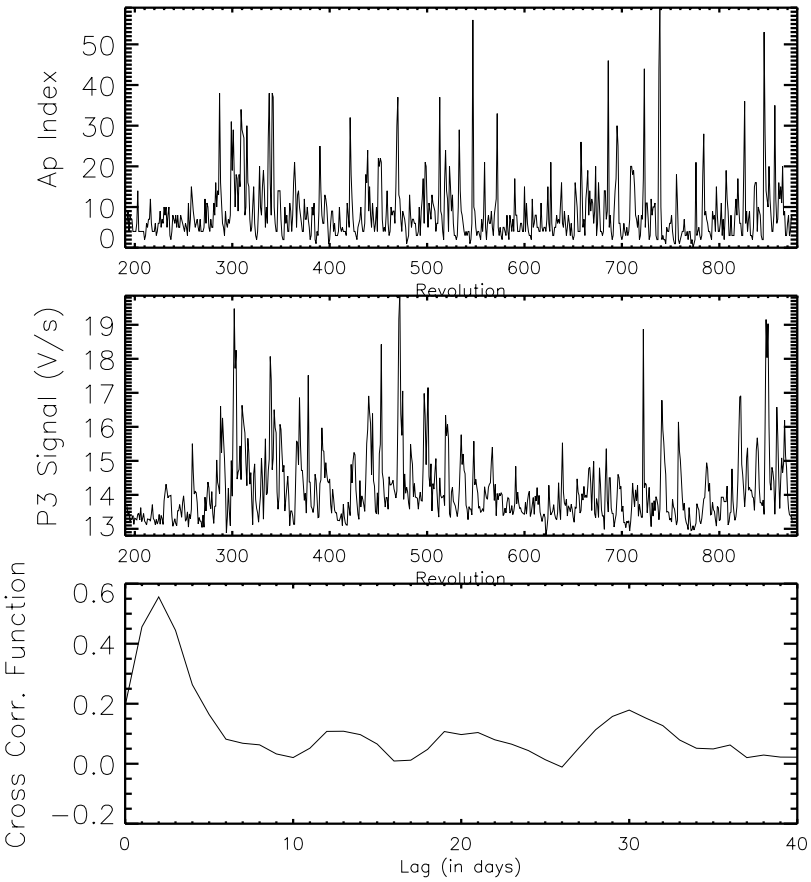

Figure 3-6 Variation of the A_p index (top panel) and o the responsivity signal for P3 (middle panel) as a function of time. In the bottom panel the cross-correlation between the A_p index and the P3 signal is shown.

3.6 Study of radiation effects on detector behaviour

The responsivity check signals of the ISOPHOT P3, C100 and C200 detectors (Ge:Ga) were clearly correlated with the geomagnetic activity and the electron fluxes (see Figure 3-6). The responsivity systematically increased one or two days after the onset of a geomagnetic storm. P3 and C100 showed the largest changes, followed by C200. Evidence of the effects of the space environment triggered by solar activity is also seen from the auto-correlations functions for P3, C100 and C200, that showed a maximum at 26-29 days, which corresponds closely to the period of solar rotation. The P1 and P2 detectors showed long period changes of signal. Further studies are required to determine if those variations might be attributed to seasonal changes in the orbit orientation of ISO with respect to the magnetosphere. For more information on the influence of the space weather on the behaviour of the ISOPHOT detectors, see Castañeda & Klaas (2000).

The periodicity found in the behaviour of the ISOPHOT detectors coincides with the one identified for the dark current variation of the ISOCAM LW detector, and which has been associated with the 27-day recurrent electron events detected by the GOES 9 spacecraft.

The dependency of ISOPHOT dark currents and responsivity on orbital phase (or position in revolution) can be analyzed by running the corresponding IA routines, as explained in C. Gabriel's note.

The space radiation environment influenced significantly the long term behaviour of the SWS band 3 Si:As detectors. The other SWS bands were not permanently affected by radiation and their dark currents, dark current noise and responsivities were stable during the whole mission (Heras et al. 2000). Most detectors in band 3 showed a continuous increase in the dark current level as a function of time. The responsivity, however, remained stable. When the dark current increased over a certain threshold, it was also associated with an increase in the dark current noise. Figure 3-7 shows, as an example, the dark current and dark noise evolution for two band 3 detectors. Detector 35 showed a dark current level increase which was not associated with a higher dark current noise. The opposite is true for detector 36, in which the dark current noise reached rather high values. In particular an increase in the "pop-corn" noise was observed (jumps of the dark current between two levels). Some of the worse band 3 detectors cured spontaneously (e.g. detectors 34 and 36), that is, their dark currents and noise decreased suddenly to launch levels without apparent reason. Laboratory tests in which Si:As detectors were irradiated with 100 MeV protons during long periods reproduced successfully the in-orbit behaviour. Although no curing procedure could be found, it was decided to operate the detector at a lower bias than initially planned, which reduced the damaging radiation effects and kept the dark currents and noise at acceptable levels during the mission.

(*Extracted and adapted from Heras et al. 2001.)*

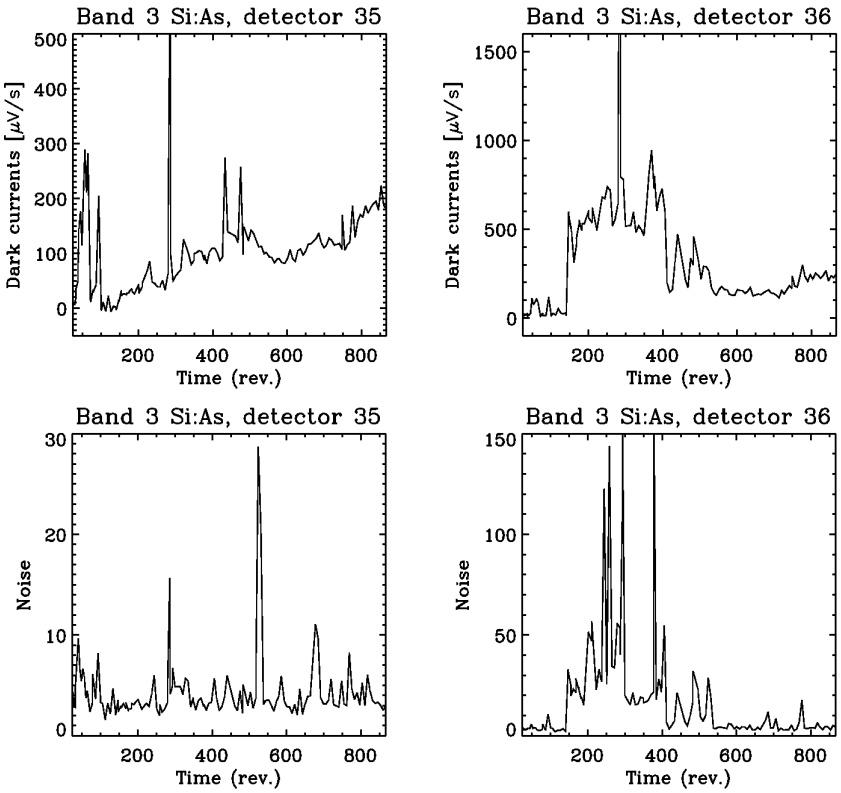

Figure 3-7 Temporal evolution of dark currents and dark current noise for two detectors of band 3.

4. Glitch detection, deglitching and detailing in IA and pipeline

4.1 ISOCAM

Due to the high energy of the GCRs, it is impossible to prevent glitch apparition with a passive shielding around the detector. It is thus necessary to develop glitch removal methods in order to get rid of them. It is important to have clear ideas about the various origins and profiles of glitches in order to be able to remove them. Several methods for glitch removal have been developed. The best ones use the multi-resolution median transform and the pattern recognition. The deglitching methods described below are implemented in CIA. In the ISOCAM pipeline deglitching is performed by median filtering of 20 exposures.

4.1.1 Manual method

Glitch can be recognized by the eye and pixels masked manually. This method is robust but of course very time consuming. It can be used as a second run after an automatic method.

4.1.2 Temporal criterion

Let m and σ be the mean and standard deviation for each pixel value $v(t)$. The temporal criterion is: if $|v(t)-m| > k\sigma$ then the pixel is considered as a glitch and is masked. This method is simple but not robust. The mean value is indeed biased due to transient behavior and glitch tail.

4.1.3 Spatial and temporal criterion

Let $cube(x,y,t)$ be a set of pixelized (x,y) images, recorded at different times t. Let $\Delta cube(x,y,t) = cube(x,y,t) - cube(x,y,t-1)$, $m(t)$ and $\sigma(t)$ be the mean and standard deviation for each frame of $\Delta cube$, $m = median(m(t))$ and $\sigma = median(\sigma(t))$. The spatial and temporal criterion is: if $\Delta cube(x,y,t) > m + k\sigma$ then the pixel is considered as a glitch and is masked. This method is relatively efficient for non stabilized data. But it is not efficient neither for long glitches (Type-B or C) nor for successive glitches in a short period of time.

4.1.4 Multi-resolution median transform

As the glitch structures can have different sizes, we need a multi-resolution tool in order to perform efficient automatic detection. The idea developed here is the following: as we observe the same position in the sky during N exposures, we cannot have any structure in the signal which has a temporal size less than NxT_{int} (T_{int} being the exposure time of a single frame). It means that all the significant structures (i.e. not due to the noise) at small temporal scales are due to glitches. The multi-resolution median transform (MMT) consists of a series of smoothing of the input image, with successively broader kernels. Each successive smoothing provides a new resolution

scale. The multi-resolution coefficient values constructed from differencing images at successive resolution scales, are not necessarily of zero mean, and so the potential artifact-creation difficulties related to this aspect of wavelet transforms do not arise. Figure 10 in Claret et al. 1999 shows the results of such a treatment.

4.1.5 Pattern recognition

In some raster observations, the signal can be modelled as a simple sum of few components: background + point sources + glitches. It is the case of main deep surveys carried out with ISOCAM. Then each component can be reconstructed separately from its multi-resolution coefficients, and can be classified following different criteria. This pattern recognition approach allows to eliminates faders and dippers in automatic and robust way, but can unfortunately not be applied to all types of data. Figure 11 in Claret et al. 1999 presents the result (bottom panel) after applying such a treatment to original data (top panel).

(the above sections 4.1.1, 4.1.2, 4.1.3, 4.1.4, and 4.1.5 have been extracted and adapted from Claret et al. 1999. See this publication and Claret et al. 2000 for further information.)

4.1.6 Innovative methods for cosmic ray rejection

The deglitching techniques explained above or sigma clipping work “blindly” on a data vector only and therefore ignore valuable information about ISOCAM’s current configuration, our knowledge of glitch distribution in time, and the current flux level per pixel. Therefore the standard deglitchers have often to rely on badly chosen thresholds, which consequently result in too high noise level due to unsuppressed glitches, masked out sources or gradients during stabilisation and no deglitching for observations with few read-outs.

In the paper “Innovative Cosmic Ray Rejection in ISOCAM Data”, S. Ott, L. Metcalfe, A. Pollock, and R. Tuffs present five new deglitching algorithms suited for different types of ISOCAM data and discuss their applicability. They also show examples demonstrating the improvements gained by these deglitching techniques.

4.1.7 Detection of faint sources and deglitching

In the “ISOCAM Faint Source Report”, B. Altieri, L. Metcalfe, S. Ott, A. Biviano, J. Blommaert and M. Delaney describe the problems related to the detection of faint sources in ISOCAM LW raster maps. These problems mainly derive from the global and glitch-induced transient responses in the time histories of the pixels. The authors describe several data processing methods that have been developed to extract point-like sources on a uniform background, and conclude that ultimate ISOCAM sensitivities which can be reached, are at least similar to pre-launch expectations. As described in the paper, the deglitch MM or PRETI methods are not perfect for deglitching, so some phase-2 deglitching on the cube of data can be attempted before building the exposures or the mosaic. Algorithms available in CIA for this purpose are:

- “spat” for a spatial deglitching

- “temp” for a temporal deglitching
- “part” for a particle analysis
- “tcor” for transient corrected deglitching
- other automatic methods, like sigma-clipping the sky-pixel history or simply manual deglitching (deglitch man), which is extremely time consuming and tedious (992 pixel time histories to examine...), but can be rewarding.

The observer should note that all currently available deglitching algorithms allow a certain fraction of glitches to get past them - for glitch characteristics not captured by the algorithm’s parameters. These residual glitches are generally clearly visible upon inspection of the deglitched data cube.

When the images at each individual raster position are averaged to produce one exposure per raster position, each such exposure may show several residual glitches. Building the mosaic from the median of these raster position exposures can help to reduce the impacts of these residual glitches on the final mosaic. Also, the cube of detector readouts (raster.cube) may be sigma-clipped. Alternatively, manual deglitching may be done (deglitch man). However, both of these techniques may attenuate real sources and should be used only with extreme caution.

More recently, aversion of phase 2 deglitching has been employed applying filters to the history of a sky pixel, and this appears to offer an alternative to manual deglitching or sigma-clipping of the detector pixel history which gives good residual-glitch rejection without significantly impacting source photometry even for bright sources.

(Extracted from “ISOCAM Faint Source Report”. See this paper for more information.)

4.2 LWS

4.2.1 Glitch detection in the LWS pipeline

This section describes the method by which glitches were detected by the LWS pipeline. The method used was a combination of both a theoretical and an empirical approach, which appeared to work well in practice. It was invented by S. Church and later modified in virtue of the experience gained during operations.

Each of the ten LWS detectors produced a series of voltage read-outs organised into ramps. The glitch detection process consisted of searching for unexpected jumps in voltage between read-outs. The first 55 msec of data at the start of each ramp were corrupted by the ramp reset process and could not be checked for glitches. The remaining read-outs in each ramp were checked for glitches as follows:

1. For each read-out two differential values were calculated. The first value was the gradient, in volts per time unit, between the read-out and the following read-out. The second value was the gradient between the read-out and the next but one readout.

2. The mean and standard deviation of the first set of differentiated points was then calculated. To help exclude values which were corrupted by glitches the two largest values in the set were excluded from this calculation.

3. Each value in the two sets of differentials were then checked using the mean and standard deviation values found above. If the differentiated value was more than 3.5 standard deviations away from the mean then it was marked as an “outlier”.

4. Glitches produce characteristic patterns of outlying points. Starting from the beginning of the ramp, the patterns were searched for and any match was regarded as a glitch. If a glitch was found, the next three points were not checked as the effects of a glitch would often cause a second false glitch detection shortly afterwards.

5. Once a glitch had been detected, its height was estimated. This was done by finding the difference between the read-out voltage at the glitch location and the read-out voltage three places ahead. We used the read-out three places ahead to help reduce the effects of noise caused by the glitch and because some glitches spanned more than one point. If the second read-out was beyond the end of the ramp then the last read-out in the ramp was used instead. The glitch height was then adjusted by subtracting the expected voltage increase between the two read-outs if no glitch had occurred.

6. The final step was to discard any glitches which were insignificant with respect to the ramp height. This helped to filter out spurious glitch detections. This was done by comparing the estimated glitch height with the height of the ramp. The height of the ramp was simply calculated as the last read-out minus the first read-out, minus the glitch height. This gives the height of the ramp as if no glitch had occurred. Glitches with a height less than 0.03 of the ramp height were rejected.

Once a glitch has been detected, the following steps are taken to remove it:

1. After a positive glitch, the rest of the ramp and the next two ramps are discarded.

2. After a negative glitch, which is almost two hundred times less frequent than a positive one, only the rest of the affected ramp is discarded. It is assumed that this kind of glitch is caused by a hit of the field-effect transistor, not the detector.

4.2.2 Deglitching with interactive data processing

The routine “inspect-spd” in the LWS Interactive Analysis (Sidher et al. 1998) allows the user to examine the contents of the LWS Standard Processed Data. In a two panel plot for each detector it shows the extracted photocurrents before and after the glitched points have been removed. It is particularly useful for demonstrating the success or otherwise of the glitch detection algorithm

described in the previous section, and for comparing the effects of glitches between different detectors. Glitch statistics are displayed to the user for each detector. The display widget allows hardcopies of plots to be made by saving output as a PostScript file.

The deglitching performed by Derive-SPD is believed to remove the majority of the glitches in the data. However, some glitches may still remain undetected as illustrated in Figure 5.1. In cases where the pipeline failed to remove glitches, this has to be done in each scan manually using the ISO Spectroscopic Analysis Package. The user can also choose to delete all data that differs by more than a given number of standard deviations from the median, thereby discarding all outliers in the spectrum.

(Extracted from Burgdorf et al. 2001.)

4.3 ISOPHOT

The ISOPHOT detector output data are integration ramps with high readout frequencies and therefore with a high data redundancy. Taking into account the fact that on average the disturbance by an individual glitch lasts for a fraction of a second, and a typical glitch frequency is one event every 10 seconds, it can be concluded that statistical analysis is a good way of eliminating glitch effects in the data. The various algorithms developed so far, which are based on statistical analysis, constitute basically of a search for deviating values within a distribution of differences between consecutive readouts or on a higher level between signals. For a constant illumination the measured signals should approximately form a gaussian distribution, whereas glitches show up as tails in such distributions. However, there are two facts to be taken into account when searching for deviant values in the signal distribution:

- the signal transient effects, which are induced by every illumination change, making the signal distribution highly non-gaussian (for a description of transient effects see Acosta et al. 2000)

- the hysteresis effect observed after a glitch, which can be described as a sudden change of responsivity with a long relaxation time.

All PIA deglitching algorithms contain three basic steps:

1. Preparation of the data for glitch detection: The detector signals may suffer from transient effects which broaden the signal distribution and therefore small level glitches cannot easily be recognized. As an attempt to minimize this effect we remove the baseline trend, for instance by using the smoothed signal sequence after applying a median filter. Another limiting effect is non-linearities in the integration ramps, especially when a large part of the available dynamical range in voltage is used. In this case the difference between consecutive readouts will reflect any uncorrected ramp non-linearity, which is modulated with the reset frequency.

2. Detection of outlying points: The average and standard deviations of the signal distribution for a constant illumination are computed, and the points outside a few standard deviations from

the average are flagged as bad. The use of minimum-maximum clipping (not using the extremes of the distribution) makes the recognition of deviant points more efficient.

3. Glitch tail recognition: Detection of the main glitches is performed very efficiently via step 2, however in most cases the tails after a strong glitch cannot be recognized in the same way. There are several ways to cope with these cases: One possibility is the iteration of step 2 eliminating the discarded values from the sample. Another possibility is to look explicitly at the signals which follow a glitch event. Those signals will be accepted only when their deviation from the mean signal falls below a second threshold, which is set to a smaller value than the one used for detecting the prime glitch event (this algorithm was originally proposed by Haas et al. 1996).

These steps are combined differently within the reduction methods currently implemented in PIA.

4.3.1 Implementation in PIA

There are two deglitching routines working on the ERD level of the data processing and one on the SRD level. The basic idea behind these algorithms is to mask all data points affected by glitches, and at the same time to keep a maximum of unaffected data. None of the algorithms try to restore the affected data. In practice, it has been shown that the use of one of these algorithms is in general sufficient to identify most of the glitches; however, the best results are obtained by the application of one correction at ERD level followed by the correction at SRD level.

4.3.1.1 Correction on ERD level

There are two ways of deglitching the data at ERD level: a simple approach which discards deviating signals above a certain threshold, and a more sophisticated approach, which identifies the glitch and also looks for a possible subsequent tail discarding deviating signals above a second threshold. After all affected readouts have been masked, the integration ramps are reconstructed by computing local mean values of the differential signal. This is done in order to use most of the unaffected data and to have a better sampling of the dynamical range of voltage. This is especially important when there are only few integration ramps within the frame of a single measurement.

1. Simple approach: This algorithm works on a per ramp basis and hence it requires a sufficient number of readouts per ramp to use statistical analysis. This means that it cannot be applied to measurements of very bright sources for which ramps contain only few readouts. The separation in ramps minimizes the possible dispersion due to signal transients. The signals are derived from consecutive readout differences and then the mean and the standard deviation (σ) of those values are computed. Several iterations (default is 4) can be done after rejecting signals deviating by more than a few σ (default is 4.5). This algorithm works very well for glitches which affect a small number of read-outs within a ramp and do not show long tails. This is the case for observations of intermediate brightness sources. See Figure 2 in *Gabriel & Acosta-Pulido (2000)* for an example.

2. Complete approach: In this second implementation differential signals are also computed from pairs of consecutive readouts but several ramps are used at once, in practise all those belonging to a constant illumination level, with the same filter and at the same sky position. This feature extends the deglitching at ERD level to those measurements with only a few readouts per ramp, which cannot be handled by the simple method. In order to minimize the scatter introduced by transient effects within the signal distribution, the temporal signal sequence is normalized by a smoothed sequence which results from applying median filtering. The basic difference w.r.t. the previous method is the use of two thresholds to detect the glitch effects: one is used for detecting the primary glitch event (default: 3σ), and the other is used for rejecting affected data following primary glitches (default: 1σ). In this way most of the tails following strong glitches can be detected. This method is well suited for observations of low flux sources when glitches produce long tails and only a small part of the voltage dynamical range is used, thus avoiding the effect of non-linearities in the integration ramp. See Figure 3 in *Gabriel & Acosta-Pulido (2000)* for an example.

4.3.1.2 SRD Level

In general both of the previously described algorithms produce reliable results, and the signals obtained after ramp fitting are relatively free of glitches. However, there are cases in which residual effects are still present. In most cases, the number of signals corresponding to a given flux level allows sensible statistics. The glitch detection is done by computing a “running mean’, which considers simultaneously a certain number of consecutive data points which are shifted along the whole measurement (the box size is configurable). An additional condition can be set stipulating that data points are considered to be affected by glitches if they are detected in different boxes (by default in two). This process can also be iterated a number of times discarding the masked points in previous iterations. This method was originally developed for the ISOPHOT Off-line Processing Pipeline (Guest, 1993), and was later adapted to get full interactive capabilities within PIA. The application of this correction to an already readout deglitched distribution is shown in Figure 4 of *Gabriel & Acosta-Pulido (2000)*, in which the signals obtained without any deglitching are also shown.

4.3.1.3 Results obtained after deglitching

Applying deglitching procedures significantly increases the data quality. Typically, an improvement of a factor of two in the signal-to-noise ratio can be achieved by the application of one deglitching procedure and up to a factor of three when combining deglitching at the ERD and SRD levels of the data reduction. The deglitching procedures vary in efficiency depending on several observing conditions, like illumination level, orbital position and space weather conditions at the time of the observation. There were only very few cases in which extreme conditions, especially strong geomagnetic storms make the data unrecoverable (Castañeda & Klaas 2000). Under such conditions the glitch frequency is as high as the readout frequency, which makes it very difficult to distinguish glitches from the voltage increase by the IR photocurrent.

Another important feature in the data reduction which helps to get rid of glitch effects is the use of “weighted means” to obtain a final signal for a given observation. Signals from ramps containing

glitches hereby get a very low weight and impact only minimally the final value. The weighting factors are the inverse of the squares of the signal uncertainties.

(Extracted from Gabriel & Acosta-Pulido 2000. See this publication for figures and further information. Its Section 5 describes the graphical interfaces provided in PIA for interactive deglitching.)

4.4 SWS

The SWS data is deglitched automatically in the pipeline as part of the derive-SPD process. How glitches are recognised in the data depends on which AOT the data is from. For AOTs 2, 6 and 7 SW grating section, the grating scanner does not move during each reset interval. Any sudden jump in the output of a detector during a reset interval is probably a glitch and can be recognised as such. For AOT 1s however, the grating does move during a detector reset interval and can scan across an entire line during a reset interval. If the line is strong enough there can be several signal jumps as the grating scans across it that can be mistaken for glitches.

4.4.1 Glitch detection in AOT 1s

Because in AOT 1s the grating is moving during a detector reset interval special care has been taken reducing the data in order not to confuse narrow lines with glitches. In order to correctly distinguish between glitches and unresolved lines, a source signal is estimated and subtracted from the ramp derivative before deglitching is carried out. This source signal estimate is derived using the knowledge that the source signal should be constant while the grating scanner is not moving (as then each detector only sees one wavelength of light). The algorithm used for glitch detection on the corrected ramp derivative is the same as used for other AOT's.

In OLP 10 false glitch detections are now highly suppressed and real glitches are still caught. In the few cases where there are still glitches detected where there should not have been one, they have little effect on the derived signal. OLP 10 AOT SWS01 data can therefore be used without any restrictions. The same applies to data reduced in the coming release (V3.0) of the SWS OSIA system.

For more information on how glitches are recognised in AOT 1 data see Lahuis, Kester and Shipman (2001).

4.4.2 Glitch detection algorithm

Glitches are recognized in the differentiated outputs of each detector. For each detector, the differentiated outputs for one reset interval are sorted and the median width of its distribution are calculated. If, for any sample, the deviation of its derivative with respect to the median is larger than ALPHA times the median width, and in absolute terms larger than MINWID, the sample is classed as a glitch. The values of ALPHA and MINWID are held in CAL-G file 6.

If any differentiated 24 Hz bit values are flagged as glitches, the samples around it are checked and, if affected, also marked. Affected here means that when the deviation of a sample (of which the neighbour is identified as a glitch) exceeds half of the nominal limit (ALPHA/2), it is also flagged as a glitch. So for neighbouring samples the threshold is lowered to effectively ~1.5 sigma instead of the normal ~3 sigma.

If the glitch is so strong that the electronics go into saturation, all measurements up to the end of the ramp will already have been discarded at the determine data range stage. Another possibility is that after a strong glitch the electronics do not saturate but the sample goes outside the 0.4096 binary limits. Then the signal will come back into the 0.4096 range after a few samples. This happens frequently and is a consequence of the high-pass filter. Then only the samples outside the binary range are flagged and dealt with as glitches in the further processing.

If glitches are detected during a reset this is noted in the flag word. An additional possibility to identify problematic ramps is the offset tag in the SPD/AAR product. This tag contains the actual number of samples contributing to the slope calculation. A third possibility is the SWS Glitch History (SWGH) file, which contains a list of all glitches detected during processing along with a short characterisation, such as glitch height. For a description of this file see section A.3.2 of ISO Handbook Volume VI.

The accuracy of deglitching depends not only on how well a glitch can be identified, but also on the effects of the glitch with time (the so called glitch-tails). Figures 4.6 and 4.7 of the ISO Handbook Volume VI show the effect of the deglitching software. Figure 4.6 is of a portion of ERD affected by glitches. Figure 4.7 shows this ERD processed to SPD both with and without the deglitching software. Where it has not been used the glitches in the ERD cause the slope in the SPD to vary rapidly in time. Where the software has been used it has identified where the glitches occur, allowing them to be taken into account when calculating the slopes. The resultant SPD is much smoother.

For a further discussion of glitches and their correction see Kester et al. (1999), and Wieprecht et al. (2000).

(Extracted and adapted from section 4.2 7 in ISO Handbook Volume VI.)

5. Implications for future missions

5.1 Introduction

The analysis of the radiation effects on the ISO data is of particular importance for the preparation of future missions, as for example SIRTF, NGST and FIRST (Herschel). The understanding of the radiation causing the glitches in the ISO data will help:

- in the building of the instruments (e.g. avoiding radioactive coatings)
- in the design of the satellite and instrument shielding,
- to provide estimates through the application of models of the glitch rates expected and their influence on the noise,
- to analyze the impact of the space weather and radiation on satellite operations (e.g. shut-down of the instruments during intense solar proton events).

In addition, future missions can benefit from the experience in the development and application of glitch detection and removal algorithms to the ISO data.

5.2 Radiation effects on the Herschel-PACS detectors

5.2.1 Introduction to the FIRST/Herschel Space Observatory mission

The Far InfraRed and Submillimetre Telescope (FIRST) (recently renamed as Herschel Space Observatory) is the European Space Agency's fourth cornerstone mission in the Horizons 2000 programme to be launched in 2007. It will perform photometry and spectroscopy in the 60-670 μm range and will be operated as an observatory for a minimum of three years in an orbit around the Lagrangian point L2, which is located 1.5 x 10^6 km away from the Earth in the antisunward direction.

FIRST (Herschel) will carry three science instruments inside a superfluid helium cryostat:

- HIFI (Heterodyne Instrument for the Far-Infrared), a very high resolution spectrometer (0-300 km/s) with a frequency coverage from 480 to 1250 GHz, from 1410 to 1910 and from 400-2700 GHz. It will make use of superconductor-insulator-superconductor (SIS) and hot electron bolometer (HEB) mixers.
- PACS (Photodetector Array Camera and Spectrometer), an imaging photometer and integral field line spectrometer for wavelengths up to ~210 μm. It has recently been redesigned to employ in total four detector arrays, two bolometer arrays for photometry, and two Ge:Ga detector arrays for spectroscopy.

- SPIRE (Spectral and Photometric Imaging REceiver), which comprises an imaging photometer and a symmetrical Mach-Zender imaging spectrometer. SPIRE has five bolometer detector arrays.

Although it is expected that the volume and nature of the bolometer detectors makes them little sensitive to the radiation environment, the extent and characterization of the radiation effects will be more precisely assessed during instrument radiation tests. On the contrary, the Ge:Ga photoconductor arrays used in the PACS spectrometer will suffer the impact of the radiation environment in a way similar to ISO's. For this reason the activities of the GWG in relation with FIRST (Herschel) have mainly been concentrated on the PACS instrument.

Initially PACS photometry was also based on photoconductor detectors. The high instrument data rate in this mode required data processing and compression, including automatic deglitching, to be done on-board. This aspect was particularly critical because of the strong effects of glitches on the photoconductor detectors. Therefore it became essential to carry out simulations in order to check the efficiency of on board data deglitching. However, the replacement of the photometry photoconductor detectors by bolometers has relaxed the criticallity of the problem. For the spectrometer, the required downlink data rate is lower, meaning that less processing and compression needs to be done on board. Consequently the deglitching treatment in spectroscopy mode will most probably be similar to the one applied to ISO.

5.2.2 Expected radiation environment during the FIRST (Herschel) mission

The radiation environment to be encountered by FIRST (Herschel) in its orbit around L2 will consist of galactic cosmic rays, solar particle events and solar and jovian electrons. FIRST launch in 2007 will coincide with the solar minimum. Therefore a small number of major solar particle events is expected during the first part of the mission. In the end of the nominal mission, 3.5 years later, the number of damaging solar proton events will have increased drastically due to the new solar maximum in 2011. Solar proton events will be particularly problematic during a possible FIRST (Herschel) extended mission.

During quite time the dominant radiation source will be the jovian electrons, characterized by a energetic population and a 13 month synodic year modulation. Solar electron will be an important source a lower energies with abrupt peak emissions, and a 27-day period modulation (also seen by ISO, see section 3.6).

The total radiation doses have been calculated by Evans (1997). In this calculation the radiation belt trapped particles (affecting FIRST during the orbit insertion trajectory) and the solar flare protons have been considered. Galactic cosmic rays have been ignored in the analysis.

5.2.3 PACS Glitch simulations

Most of the PACS glitch simulations were performed under the assumption that photoconductor detectors would be used in photometry mode. Since these detectors have been replaced by bolometers, most of the calculations are obsolete. However the glitch rate calculations are still valid for the spectroscopy mode. In this case the background will be 1000 times lower than in photometry mode, making the glitch size larger in relation with the continuum.

The number of days in which the observations will be strongly affected by glitches has been calculated taking into account the characteristics of the PACS photoconductor detectors, the frequency of intense solar proton events during solar maximum and minimum (see figure here), and the proton and alpha particles spectra and fluence for large events (see figure here). It is estimated that 20 days per year of overwhelming proton flux will occur during solar maximum, during which no PACS spectroscopy mode observations will be possible.

The glitch rate in the bolometers has been estimated by the group responsible for their development as 1 hit per minute. This value must be taken as preliminary since the actual characteristics of these detectors are not yet precisely known. The effects of large proton events on the bolometers have not been analyzed yet.

5.2.4 The SREM radiation monitor for FIRST (Herschel)

Our understanding of the radiation affecting the ISO detectors is limited by the lack of detailed knowledge of the radiation conditions around the spacecraft. Independent measurements of the incident particle fluxes of protons and electrons would have provided extremely valuable information to assess the accuracy of the models, to understand the effects of the shielding and to better determine the nature of the particles affecting the detectors. In order to improve the situation for FIRST (Herschel), the GWG has been discussing the possibility to include a radiation monitor in the satellite, in particular a Standard Radiation Monitor (see http://pc1582.psi.ch/SREM). Some of the characteristics of the currently existing SREM are:

- Detection of protons from 10 MeV to hundreds of MeV, and electrons in the energy range 0.3-5 MeV.
- Provision of a radiation alarm flag.
- 1 internal and 6 external dosemeters
- Weight 2.5 kg, power consumption 2.6 W, volume 2 litres
- It has been or is going to be implemented in several missions: STRV-1c, INTEGRAL, SMART-1, Rosetta, ISS

The GWG has concluded to recommend the integration of a SREM in the FIRST (Herschel) satellite (see section 5.3). The current situation is that provision has been made in the System Requirements Specification of the ITT for the FIRST (Herschel) Prime contractor to provide a SREM

monitor. It has to be taken into account that the radiation monitors are evolving and by the time FIRST (Herschel) is launched a new generation will be available. In particular, new instruments in the mass range 100 g - 1.3 kg are under development.

An important aspect for FIRST (Herschel) is the data rate that a radiation monitor requires, which should be in any case well below 1 kbit/s. Although it depends on the accumulation time, the data rate of the SREM currently used on the STRB satellite, for example, is 160 bits/s, a value acceptable for FIRST (Herschel).

It must be ensured that the radiation monitor to be integrated in FIRST (Herschel) detects the type of particles and in the energy ranges that affect the FIRST (Herschel) detectors. This implies that the radiation monitor must be tailored depending on the results of the radiation tests of the FIRST (Herschel) instruments.

It is an open issue whether the radiation monitor should send an alarm to the OBDH when a severe solar proton event occurs, to trigger an automatic switch off of the instruments.

5.3 Recommendations

The ISO/FIRST Glitches Working Group, based on the ISO experience, makes the following recommendations for future missions:

1. The GWG agrees in recommending to the FIRST (Herschel) Project the inclusion in the FIRST (Herschel) satellite of the Standard Radiation Environment Monitor (SREM), or the future MRM, in order to have independent measurements of the radiation environment which will be of fundamental importance for the understanding of the radiation effects on the FIRST (Herschel) instruments (especially PACS).

2. The radiation monitor should be tailored to detect those particles and in those energy ranges that affect the FIRST (Herschel) detectors according to the instrument radiation tests.

3. Ground radiation tests are mandatory to test the detector response and compare it to the predicted one, to verify the background calculations and to confirm that deglitching and other algorithms for radiation background removal operate correctly.

4. In addition to the experimental radiation testing, detailed and critical particle simulation analysis should be carried out before launch. The ESA de facto standard for this type of studies is the GEANT4 Monte Carlo toolkit. It is also possible to adapt the ISOCAM Monte-Carlo simulation tool (Claret and Dzitko 2001b), both for photoconductors and bolometer detectors.

5. The estimates of glitch rates and the models and simulations of glitches in the science data must consider not only protons, but also electrons and secondary particles and δ-rays produced in the detectors and in the shield.

6. The combined use of laboratory radiation test data, results from simulations and existing glitch databases (e.g. ISO) is strongly recommended to simulate and understand the radiation effects on the science data, both during quiet periods and during intense solar proton events. This will be extremely useful for a better pre-launch estimate of the Signal-to-Noise ratios, for the development and testing of deglitching algorithms and to define appropriate strategies for instrument operations in relation with space weather events.

7. It is recommendable for future infrared missions, notably for FIRST (Herschel), that shielding data be calculated in the sensitive detector locations, but without any thickness limits such as in the ISO shielding data matrix. Ideally, however, for accurate Monte Carlo analysis the best solution is to construct a geometrical model representing the detector and spacecraft structure in which the particles can be transported. For this purpose, it is vital that material, geometry and dimensional information at all levels of the spacecraft are maintained in computer-readable form.

8. The design of the instrument shielding must take into account the production in the shield of secondary particles and δ-rays, since they can be a large fraction of the observed glitch rates in the science data. That is, adding more shielding material around the detectors and other sensitive elements in not always beneficial

9. The materials used to built an instrument must be checked for radioactivity, since it can contribute significantly to the observed glitch rates. For example, the anti-reflection coating of lenses in ISOCAM contained ^{232}Th, which generated a flux of low energy α-particles. At its maximum value for the 12 arcsec/pixel lens, its contribution to the observed glitch rate was equivalent to the galactic cosmic ray's.

10. It must be kept in mind that more than once an unexpected, radiation-related "surprise element" has been discovered either just before or during a mission (e.g. in Chandra and XMM-newton missions). One should not ignore this possibility, even in cases where allegedly radiation-tolerant technologies are used.

6. References

Acosta-Pulido J. A., Gabriel C., Castañeda H. O., 2000, *Transient Effects in ISOPHOT Data: Status of Modelling and Correction Procedures*, Experimental Astronomy 10, 333

Agnese P., Engelmann J.J., Mottier P., 1991, *Results of Radiation Tests Performed on the ISOCAM Infrared Detector Array*, IEEE Trans. on Nucl. Sci. 38, 953

Altieri B., Metcalfe L., Ott S., Biviano A., Blommaert J., Delaney M., 1998, *ISOCAM Faint Source Report*, ISOCAM internal document

Apostolakis J. et al., 2001, in preparation, website http://wwwinfo.cern.ch/asd/geant4/geant4.html

Burgdorf M., Harwood A., Sidher S., 2001, *Radiation Effects on LWS Detectors and Deglitching of LWS Data.* In: Proceedings of "The Calibration Legacy of the ISO mission", L. Metcalfe et al. (eds), ESA SP-481, in press

Castañeda H. O., Klaas U., 2000, *Recognition of Space Weather Impact on the ISOPHOT detectors*, Experimental Astronomy 10, 369

Chauvie S. et al., 2001, NIM B, submitted, website http://www.ge.infn.it/geant4/lowE/

Claret A., Dzitko H., Engelmann J.J., 1999, *Transient particle effects on the ISOCAM instrument on-board the Infrared Space Observatory*, IEEE Trans. on Nucl. Sci. 46, 1511

Claret A., Dzitko H., Engelmann J., Starck J.-L., 2000, *Glitch effects in ISOCAM Long Wave detector*, Experimental Astronomy 10, 305

Dzitko H., Claret A., Engelmann J., 2000, *Cosmic Ray Effects on the ISOCAM Long Wave Detector*, Experimental Astronomy 10, 279

Claret A., Dzitko H., 2001a, *Understanding and modeling glitch effects in ISOCAM*. In: Proceedings of "The Calibration Legacy of the ISO mission", L. Metcalfe et al. (eds), ESA SP-481, in press

Claret A., Dzitko H., 2001b, Experimental Astronomy, in preparation

Eckardt S., 1999, Ph. D. Thesis

Evans H., 1997, *FIRST L-2 Radiation Environment*, esa/estec/wma/he/FIRST/3

Evans H., 1998, *Space Radiation Environment during ISO mission*, esa/estec/ema/he/ISO/98-1

Gabriel C., Acosta-Pulido J. A., 2000, *Deglitching methods by the ISOPHOT Interactive Analysis (PIA)*, Experimental Astronomy 10, 319

GEANT, Detector Description and Simulation Tool, Application Software Group, Computing and Networks Division, CERN, October 1994

Guest S., 1993, *Deglitching of ISOPHOT Data*, ISOPHOT internal document

Haas M., Beckwith S., Meyer M., 1996, *A new deglitching algorithm for ISOPHOT*, ISOPHOT internal document

Heras A.M, Burgdorf M., Castañeda H., Claret A., Dzitko H., Ewart E., Gabriel C., Nieminen P., 1999, *The ISO detectors and the space radiation environment*. In: ESA Workshop on Space Weather, ESA WPP-155, ESA Publications Division, Noordwijk, p. 283

Heras A.M., Wieprecht E., Feuchtgruber H., Lahuis F., Leech K., Lorent R. Morris P.W., Salama A., Vandenbussche B., 2000, *The ISO-SWS detectors: Performance trends and space radiation effects*, Experimental Astronomy 10, 177

Heras A.M., Wieprecht E., Nieminen P., Feuchtgruber H., Lahuis F., Leech K., Lorent R. Morris P.W., Salama A., Vandenbussche B., 2001, *Summary of the SWS detector radiation effects.* In: Proceedings of “The Calibration Legacy of the ISO mission”, L. Metcalfe et al. (eds), ESA SP-481, in press

Kester D., et al., 1999, *Straight Lines*. In ‘Maximum Entropy and Bayesian Methods’, W. van der Linden et al. (eds), Kluwer Acad. Pub., 179

Lahuis F., Kester D., Shipman R., 2001, *Deglitching of SWS low resolution data*. In Proceedings of “The Calibration Legacy of the ISO mission”, L. Metcalfe et al. (eds), ESA SP-481, in press

Lemke. D., Klaas U., Abolin J. et al., 1996, *ISOPHOT - capabilities and performance,* A&A 315, L64

Moret-Bailly O., Julliet J.J., 1989, *ISO System Radiation Analysis*, ISO AS 14 TN 0169, Aerospatiale

Nieminen P., Sörensen J., 2000, *ISOCAM Long Wave Detector Glitches: Data and Ray-Tracing Simulations*, Experimental Astronomy 10, 381

Nieminen P., 2001, *The in-orbit radiation environment and its effects on space-borne instrumentation.* In: Proceedings of “The Calibration Legacy of the ISO mission”, L. Metcalfe et al. (eds), ESA SP-481, in press

Ott S., Metcalfe L., Pollock A., Tuffs R., 2000, *Innovative Cosmic Ray Rejection in ISOCAM Data*, ISOCAM internal document

Sidher S.D., Swinyard B.M., Harwood A.S. et al., 1998, *The LWS Interactive Analysis Software.* In: Proceedings of the First ISO Workshop on Analytical Spectroscopy, A.M. Heras et al. (eds), ESA SP-419, 297

Swinyard B., Clegg, P., Leeks, S., Griffin, M., Lim, T., Burgdorf, M., 2000, *Space Operation and Performance of Doped Germanium Photo-Conducting Detectors in the Far Infrared: Experience from the ISO LWS*, Experimental Astronomy 10, 157

Truscott P. et al., 2001, in preparation, website
http://www.space.dera.gov.uk/space_env/geant-mn.html

Tylka, A.J., et al., 1997, *CREME96: A revision of the Cosmic Ray Effects on Micro-Electronics Code*, IEEE Transactions on Nuclear Science 44, 2150

Wieprecht E., Wiezorrek E., Haser L., 2000, *SWS-Detector Glitch Effect Correction*, Experimental Astronomy 10, 199